

1 **Apolipoprotein E controls Dectin-1-dependent development of monocyte-derived alveolar
2 macrophages upon pulmonary β -glucan-induced inflammatory adaptation**

3 Theobald H.^{1*}, Bejarano D.A.^{1*}, Katzmarski N.^{1*}, Haub J.^{1*}, Schulte-Schrepping J.^{2,3}, Yu J.¹, Bassler
4 K², Ćirović B.¹, Osei-Sarpong C.⁴, Piattini F.⁵, Vornholz L.^{6,7}, Yu X.⁸, Sheoran S.¹, Al Jawazneh A.^{9,10},
5 Chakarov S.¹¹, Haendler K¹², Brown G.D.¹³, Williams D.L.¹⁴, Bosurgi L.^{9,10}, Ginhoux F.^{11,15}, Ruland
6 J.^{6,7}, Beyer M.⁴, Greter M.⁸, Kopf M.⁵, Schultze J.L.^{2,3,12}, Schlitzer A.¹

7 ¹Quantitative Systems Biology, Life & Medical Sciences Institute, University of Bonn, Bonn, Germany

8 ²Genomics & Immunoregulation, Life & Medical Sciences Institute, University of Bonn, Bonn, Germany

9 ³Systems Medicine, Deutsches Zentrum für Neurodegenerativen Erkrankungen (DZNE), Bonn, Germany

10 ⁴Molecular Immunology in Neurodegeneration, German Center for Neurodegenerative Diseases, Bonn,
11 Germany

12 ⁵Institute of Molecular Health Science, ETH Zürich, Zürich, Switzerland

13 ⁶Institute of Clinical Chemistry and Pathobiochemistry, School of Medicine, Technical University of Munich,
14 Munich, Germany

15 ⁷TranslaTUM, Center for Translational Cancer Research, Technical University of Munich, Munich, Germany

16 ⁸Institute of Experimental Immunology, University of Zurich, Zurich, Switzerland

17 ⁹I. Department of Medicine, University Medical Center Hamburg-Eppendorf, 20246 Hamburg, Germany

18 ¹⁰Protozoa Immunology, Bernhard Nocht Institute for Tropical Medicine, Hamburg, Germany

19 ¹¹Shanghai Institute of Immunology, Shanghai JiaoTong School of Medicine, Shanghai, China

20 ¹²PRECISE Platform for Genomics and Epigenomics at DZNE, University of Bonn, Bonn, Germany

21 ¹³MRC Centre for Medical Mycology, University of Exeter, Exeter, UK

22 ¹⁴Department of Surgery and Center for Inflammation, Infectious Disease and Immunity, James H. Quillen
23 College of Medicine, East Tennessee State University, Johnson City, United States.

24 ¹⁵Singapore Immunology Network, Agency for Science, Technology and Research, Singapore

25 ^{*}Equally contributed

26 Correspondence to: andreas.schlitzer@uni-bonn.de

27 **Keywords:** Alveolar macrophages, monocytes, Dectin-1, Apolipoprotein E, Pulmonary Inflammation

28

29

30 **Summary**

31 The lung is constantly exposed to the outside world and optimal adaptation of immune responses is crucial for
32 efficient pathogen clearance. However, mechanisms which lead to the functional and developmental adaptation
33 of lung-associated macrophages remain elusive. To reveal such mechanisms, we developed a reductionist model
34 of environmental intranasal β -glucan exposure, allowing for the detailed interrogation of molecular mechanisms
35 of pulmonary macrophage adaptation. Employing single-cell transcriptomics, high dimensional imaging and flow
36 cytometric characterization paired to *in vivo* and *ex vivo* challenge models, we reveal that pulmonary low-grade
37 inflammation results in the development of Dectin-1 - Card9 signaling-dependent monocyte-derived
38 macrophages (MoAM). MoAMs expressed high levels of CD11b, ApoE, Gpnmb and Ccl6, were glycolytic and
39 produced large amounts of interleukin 6 upon restimulation. Myeloid cell specific ApoE ablation inhibited
40 monocyte to MoAM differentiation dependent on M-CSF secretion, promoting MoAM cell death thus impeding
41 MoAM maintenance. *In vivo*, β -glucan-elicited MoAMs limited the bacterial burden of *Legionella*
42 *pneumophila* post infection and ameliorated fibrosis severity in a murine fibrosis model. Collectively these data
43 identify MoAMs that are generated upon environmental cues and ApoE as an important determinant for lung
44 immune resilience.

45 **Introduction**

46 The lung is the body's largest surface to interface with the outside world and is exposed to a variety of
47 immunostimulatory agents shaping the lung's ability to mount immune responses (Kopf et al., 2014). However,
48 how such environmental non-clinically apparent immune activation is controlled on the cellular and molecular
49 level is poorly understood. β -glucans are integral components of environmental pathogenic and non-pathogenic
50 fungi and have been proposed as major systemic immune modulators (Divangahi et al., 2021). Furthermore,
51 ambient concentrations of β -glucan, have been shown to oscillate over the course of the year and in combination
52 with pathogen exposure have been correlated to an increase in allergic rhinitis (Shah and Panjabi, 2014). The
53 recognition of β -glucan by Dectin-1 is crucial to modulate systemic immune responses through a process termed
54 innate immune memory (Quintin et al., 2012), characterized by increased cytokine responses of trained innate
55 immune cells, such as monocytes, upon a secondary non-related stimulus, facilitated by a metabolic and
56 epigenetic rewiring, allowing a more efficient first line immune response (Arts et al., 2016a; Arts et al., 2016b;
57 Bekkering et al., 2018; Cirovic et al., 2020; Quintin et al., 2012; Saeed et al., 2014). However, the mechanisms
58 by which β -glucan asserts its actions on the lung, the organ where it is most often recognized, and how it acts as
59 a non-genetic modifier of immune response to subsequent disease, remain unknown.

60 The immune cell compartment of the -alveolar space of the lung is the body's respiratory first line of defence,
61 ensuring efficient immune response induction against airborne pathogens, while regulating immune activation to
62 ensure intact lung function (Hussell and Bell, 2014). Within the -alveolar space alveolar macrophages (AM) and
63 monocytes constitute the major mononuclear phagocytes found during homeostasis in humans and mice. Both
64 AMs and monocytes express high amounts of Dectin-1 and exert highly plastic immune responses within the -
65 alveolar compartment (Brown, 2005). Dectin-1 signalling has been shown to depend critically on spleen
66 tyrosine kinase (Syk) which upon activation can trigger phospholipase C gamma 2 (PLC γ 2) dependent calcium
67 release and downstream nuclear factor of activated T-cells (NFAT) and extracellular signal-regulated kinase
68 (ERK) activation. This signalling cascade leads to production of interleukin (IL) 2 and 10. Furthermore Syk can
69 activate CARD9 leading to proinflammatory nuclear factor kappa-light-chain-enhancer of activated B cells
70 (NF κ B) signalling and the release of tumor necrosis factor alpha (TNF α) and IL-6. Additionally, Dectin-1
71 ligation has been described to directly induce reactive oxygen species (ROS) production via the activation of
72 phosphoinositide 3 kinase (PI3K) (Gross et al., 2006; Vornholz and Ruland, 2020). Murine homeostatic AMs
73 are embryonically derived with only minor contribution of adult bone marrow homeostasis (Guilliams et al.,
74 2013; Schneider et al., 2014). However, viral infection or radiation of the lung have been shown to induce

75 differentiation of Ly6c⁺ monocytes into long-lived monocyte-derived macrophages (Aegerter *et al.*, 2020;
76 Gibbings *et al.*, 2017; Machiels *et al.*, 2017). During viral infection monocyte-derived AMs have been shown to
77 be crucial for the defence against subsequent *Streptococcus pneumoniae* infections through increased release of
78 IL-6 (Aegerter *et al.*, 2020). Finally, environmental adaptation through viral exposure was also shown to affect
79 the interaction between resident AMs and CD8⁺ T-cells, allowing a more efficient bacterial clearance of the
80 latter upon viral training (Yao *et al.*, 2018). Chronic lung diseases, such as asthma, idiopathic lung fibrosis or
81 chronic obstructive pulmonary disease can be driven and accelerated by environmental factors. Therefore, it is
82 crucial to understand the cellular, functional and molecular consequences of the immune recognition of ambient
83 stimuli, such as β -glucan, and how the homeostatic broncho-alveolar resident mononuclear phagocyte
84 compartment adapts in origin and function (Kaur *et al.*, 2015; Lloyd and Marsland, 2017; Murdoch and Lloyd,
85 2010; Rabe and Watz, 2017).

86 Therefore, to investigate the impact of a non-pathological sterile environmental stimulus in a controlled manner
87 we developed a reductionist model of a single low dose intranasal β -glucan exposure. Using single-cell
88 transcriptomic, *in vivo* and *ex vivo* functional analysis of cellular development and downstream immune
89 responses, this model allowed us to monitor acute and long-term effects on the broncho-alveolar mononuclear
90 phagocyte compartment, and to dissect the molecular adaptation of macrophages upon environmental cues. We
91 show that a single intranasal exposure to β -glucan induces the development of functionally modified monocyte-
92 derived Apolipoprotein E (ApoE)⁺CD11b⁺ AMs, which are detected up to 21 days post β -glucan exposure.
93 ApoE⁺CD11b⁺ AMs are glycolytic and release, upon restimulation with lipopolysaccharide (LPS), high amounts
94 of IL-6. Furthermore, prior environmental adaptation by β -glucan followed by infection with *Legionella*
95 *pneumophila* or a challenge by bleomycin-induced fibrosis led to an improved outcome after the secondary
96 challenges. Molecularly, development of β -glucan induced ApoE⁺CD11b⁺ AM is controlled by the Dectin-1 -
97 Card9 signalling pathway whereas maintenance of ApoE⁺CD11b⁺ AMs depends on paracrine ApoE and
98 macrophage colony stimulating factor (M-CSF). Taken together, we identify the Dectin-1 - Card9 and ApoE
99 pathways as critical regulators of functional environmental adaption of pulmonary mononuclear phagocytes and
100 reveal the molecular constituents of such adaption processes, allowing potential future pharmaceutical
101 intervention.

102

103 **Results**

104 *Intranasal β-glucan exposure generates environmentally adapted ApoE⁺CD11b⁺ alveolar macrophages within*
105 *the broncho-alveolar space.*

106 The lung is constantly exposed to the outside world, including pollutants, sterile and non-sterile pathogens and
107 components thereof. However, knowledge about cellular and molecular mechanisms contributing to immune
108 adaptation towards such environmental cues remains scarce. To reveal such mechanisms, we designed a
109 reductionist model of a single low-dose particulate intranasal β-glucan exposure (200 µg) emulating
110 environmental exposure (Rathnayake et al., 2017). To analyse the impact of this stimulation and to probe the
111 longevity of its impact we assayed the macrophage compartment in the broncho-alveolar lavage fluid (BALF)
112 (CD45⁺Lin⁻SSC^{int-hi}) of PBS or β-glucan treated C57BL/6 mice seven days after inoculation using single-cell
113 transcriptomics (**Figure 1A, S1A-C**). Dimensionality reduction by uniform-manifold approximation and
114 projection analysis (UMAP) and unsupervised clustering using the Louvain algorithm revealed a total of five
115 transcriptionally distinct clusters in the murine broncho-alveolar compartment (**Figure 1A, B**). High expression
116 of the lung macrophage signature genes *SiglecF* and *Itgax* demonstrated that all investigated cells were of the
117 macrophage lineage (**Figure S1D, E**) (Yu et al., 2017). Further analysis identified Clusters 0 and 1 as two
118 subsets of resident AMs expressing *Ear2*, *Wfdc21* and *Fabp4*, *Hmox1*, respectively (Gautier et al., 2012; Yu et
119 al., 2017). Cluster 2 presented with expression of genes associated to proliferative processes such as *Top2a*,
120 *Mki67* and *Birc5* and was therefore termed proliferating AMs (Cohen et al., 2018). Cluster 3 (ApoE⁺ AM)
121 expressed many genes previously associated to a lipid-associated inflammatory monocyte-derived macrophage
122 phenotype such as *Apoe*, *Cd63*, *Spp1*, *Gpnmb* and *Trem2* (Aegerter et al., 2020; Jaitin et al., 2019; Keren-Shaul
123 et al., 2017). Lastly, cluster 4 (ISG⁺ AM) was marked by expression of interferon-stimulated genes (ISG), such
124 as *Ifit2*, *Ifit3*, *Ifit204* and *Isg15* (**Figure 1B**). Next, to understand whether one of the identified clusters was
125 associated with β-glucan-induced environmental adaptation, we analysed the relative contribution of each
126 condition to the clusters (**Figure 1C-E, S1F**). This revealed that ApoE⁺ AMs were only found within the
127 broncho-alveolar space of mice exposed to β-glucan seven days prior, alongside a reduction of proliferating
128 AMs. Previous work indicated CD11b expression on AMs post stimulation as a marker of enhanced
129 inflammatory potential (Halstead et al., 2018; McCubrey et al., 2018). Therefore, we utilized co-detection by
130 indexing (CODEX) enabled high-dimensional imaging (Goltsev et al., 2018) to further describe the protein-
131 level phenotype of ApoE⁺ AMs in the lung seven days post β-glucan stimulation (**Figure 1F**). This revealed that
132 ApoE⁺ AMs co-expressed classical AM markers, such as CD11c and SiglecF, but also expressed significant

133 amounts of CD11b, ApoE and GPNMB (**Figure 1F**). Therefore, we term this AM subpopulation ApoE⁺CD11b⁺
134 AMs. To further investigate the cellular dynamics of ApoE⁺CD11b⁺ AMs upon β -glucan induced environmental
135 adaptation we monitored the BALF 0-21 days post β -glucan exposure using flow cytometry (**Figure 1G, S1G,**
136 **H**). Flow cytometric analysis of the broncho-alveolar compartment showed that, in alignment with the single-
137 cell transcriptomic data (**Figure 1E**), ApoE⁺CD11b⁺ AMs peaked at day seven post β -glucan inoculation and
138 slowly diminished until day 21 (**Figure 1G**). Furthermore, in alignment with these data we found an overall
139 increase in total AMs peaking at day seven post β -glucan exposure (**Figure S1H**). Next we verified
140 ApoE⁺CD11b⁺ AMs within complete lung single cell suspension alongside their upregulated level of Siglec F,
141 confirming their AM identity (**Figure S1I, J**).

142

143 *ApoE⁺CD11b⁺ AMs are monocyte-derived and CCR2-dependent.*

144 Previous data indicated that acute and chronic inflammation can lead to the recruitment of monocyte-derived
145 macrophages into the broncho-alveolar space (Aegerter *et al.*, 2020; McCubbrey *et al.*, 2018; Mould *et al.*,
146 2017). To understand whether β -glucan induced environmental adaptation rewrites a resident alveolar
147 macrophages subpopulation or leads to recruitment of Ly6c⁺ monocytes and their subsequent differentiation into
148 ApoE⁺CD11b⁺ AMs we first monitored the influx of Ly6c⁺ monocytes in the broncho-alveolar space using flow
149 cytometry. This revealed that post β -glucan stimulation Ly6c⁺ monocytes were recruited to the broncho-alveolar
150 space peaking on day three after stimulation, remaining high ad day 7 and decreasing from day 14 onwards
151 (**Figure 2A**). To connect this data with the emergence of ApoE⁺CD11b⁺ AMs we employed the *Ms4a3-*
152 *cre*^{Rosa26TOMATO} mouse model which allows genetic lineage tracing of the bone marrow derived monocyte
153 lineage. Genetic lineage tracing revealed that 71% \pm 10% ApoE⁺CD11b⁺ AMs were labelled with tomato
154 indicating an overall bone marrow monocyte origin (**Figure 2B, C**). Additionally, CODEX imaging revealed
155 co-expression of CD11b and dtTomato in SiglecF⁺CD11c⁺ AMs within the lung, further adding weight to their
156 monocyte origin (**Figure 2D**). To further validate this finding we employed the CCR2^{-/-} mouse model in which
157 recruitment of Ly6c⁺ monocytes upon inflammation is strongly decreased (Serbina and Pamer, 2006). To
158 determine whether generation of environmental adaptation induced ApoE⁺CD11b⁺ AMs is CCR2 dependent, we
159 inoculated either control or CCR2^{-/-} mice with β -glucan and analysed the BALF seven days later using flow
160 cytometry (**Figure 2E**). This analysis revealed a significant reduction of ApoE⁺CD11b⁺ AMs upon β -glucan
161 inoculation in CCR2^{-/-} mice. Taken together these results demonstrate that β -glucan-induced ApoE⁺CD11b⁺
162 AMs arise from bone marrow progenitors in a CCR2-dependent fashion.

163

164 *β-glucan-elicited environmental adaptation increases Ly6c⁺ monocyte differentiation within the bone marrow.*

165 Systemic β -glucan administration can lead to changes in abundance and functional priming of myeloid-
166 associated precursors within the bone marrow (Kalafati *et al.*, 2020; Mitroulis *et al.*, 2018). To reveal whether or
167 not local broncho-alveolar adaptation elicits systemic feedback mechanisms affecting bone marrow
168 monopoiesis, we analysed abundance of Ly6c⁺ monocytes in blood and bone marrow seven days post intranasal
169 β -glucan stimulation using flow cytometry. Here, we found a significant reduction of both percentage and
170 absolute cell count of Ly6c⁺ monocytes in blood and an increased percentage and number of Ly6c⁺ monocytes
171 within the bone marrow (**Figure 2F-I**). To understand if the increased number of bone marrow Ly6c⁺
172 monocytes is a function of an increased precursor reservoir, we analysed the bone marrow resident common
173 monocyte progenitor (cMOP) repertoire of mice stimulated intranasally with β -glucan or PBS seven days
174 before. This revealed that activated cMOPs, expressing MHC2, were decreased in mice pre-treated with β -
175 glucan (**Figure 2J, K**). Thereby these data indicate that enhanced generation of Ly6c⁺ monocytes upon
176 intranasal β -glucan mediated environmental adaptation evokes MHC2⁺ cMOP-mediated differentiation to allow
177 generation of sufficient peripheral Ly6c⁺ monocytes. Furthermore, we addressed whether enhanced peripheral
178 demand for Ly6c⁺ monocytes and their progenitors affect the abundance of granulocyte macrophage progenitors
179 (GMP) in the bone marrow of mice intranasally stimulated with β -glucan or PBS. Here, we found a trend
180 towards reduced GMP numbers in the bone marrow of mice seven days after treatment with β -glucan compared
181 to PBS (**Figure 2L**). Taken together, these data indicate a peripheral feedback mechanism which draws upon
182 immediate monocyte progenitors to fill up demand of monocytes within the lung, without significantly affecting
183 the myeloid differentiation cascade *per se*.

184

185 *ApoE⁺CD11b⁺ AMs show increased release of interleukin 6 and induction of glycolysis.*

186 Monocyte-derived macrophages have been associated with enhanced inflammatory response after strong
187 inflammatory and infectious events, such as influenza A infection (Aegerter *et al.*, 2020). However, if and how
188 the mononuclear cell repertoire of the broncho-alveolar space functionally adapts to low grade inflammatory
189 stimuli, remains unclear. To investigate whether BALF-resident macrophages exhibit a different functional
190 profile seven days post β -glucan exposure, we isolated BALF-resident immune cells, enriched for macrophages
191 by adherence, and re-stimulated macrophages with PBS or LPS for 24h *in vitro*. Next, supernatants were
192 investigated for IL-6 and TNF α release using ELISA. This revealed that macrophages pre-treated with β -glucan

193 released significantly higher amounts of IL-6 and a trend towards more TNF α after LPS re-stimulation as
194 compared to PBS pre-treated with PBS (**Figure 3A, S2A**). To further validate that indeed ApoE $^+$ CD11b $^+$ AMs
195 were endowed with a higher capacity to release IL-6 post β -glucan stimulation, we utilized intracellular flow
196 cytometric analysis of IL-6 secretion after LPS or PBS restimulation. Here, we found a strong increase in IL-
197 6 $^+$ CD11b $^+$ AMs post β -glucan exposure as compared to the PBS exposed controls (**Figure 3B, C, S2B, C**). Our
198 data shows that generation of ApoE $^+$ CD11b $^+$ AMs upon β -glucan exposure is CCR2-dependent (**Figure 2C**).
199 Therefore, to validate that the increased IL-6 within *ex vivo* restimulated BALF resident macrophage cultures
200 can be attributed directly to ApoE $^+$ CD11b $^+$ AMs, we exposed CCR2 $^{-/-}$ and control mice to β -glucan and seven
201 days later enriched macrophages from the BALF by adherence and restimulated adherent cells with LPS for
202 24hs *in vitro* (**Figure 3D**). This analysis revealed that the increased amount of IL-6 seen in β -glucan-exposed
203 broncho-alveolar macrophages is CCR2-dependent, showing that ApoE $^+$ CD11b $^+$ macrophages are the major
204 source of increased IL-6 upon β -glucan-induced environmental adaptation. Furthermore, enhanced cytokine
205 responses upon systemic β -glucan stimulation have been linked to the induction of glycolysis within
206 mononuclear phagocytes (Arts *et al.*, 2016b; Bekkering *et al.*, 2018). To understand whether this was also true
207 in our system, we utilized extracellular flux analysis to measure glycolysis. This analysis showed that
208 glycolysis, glycolytic capacity and reserve were significantly increased on day seven post β -glucan exposure in
209 adherence-selected BALF-resident macrophages (**Figure 3E, F, S2D, E**). Collectively, these data indicate an
210 enhanced proinflammatory potential of ApoE $^+$ CD11b $^+$ AMs.

211

212 *β -glucan-induced environmental adaptation enhances pulmonary bacterial clearance and ameliorates*
213 *bleomycin induced fibrosis.*

214 Optimal adaptation to outside stimuli received via ambient air is essential for a potent, yet measured immune
215 response. IL-6 has been indicated to be a major component of an adapted pulmonary immune response. As
216 ApoE $^+$ CD11b $^+$ AMs produced increased amounts of IL-6, we wondered whether those cells have an impact on
217 the outcome of an acute and chronic inflammation. To dissect whether this enhanced cytokine secretion ability
218 affects protection against a bacterial pathogen, we utilized C57B/L6 mice, which were environmentally adapted
219 for seven days, infected these mice intratracheally with *Legionella pneumophila* and analysed the bacterial
220 burden and cellular composition of the BALF two days post infection (**Figure S3A**). Here, environmentally
221 adapted mice showed a significant decrease of bacteria detected within their BALFs and an increased count of
222 proinflammatory macrophages associated to bacterial clearance (**Figure 4A, B**). Next, to investigate if

223 environmental adaptation has consequences beyond the modulation of acute bacterial infection, we inoculated
224 environmentally adapted or control mice intratracheally with bleomycin to induce experimental lung fibrosis
225 (**Figure S3B**). Here, environmentally adapted mice showed a significantly higher rate of survival over a 14-day
226 observation period post bleomycin inoculation alongside a trend towards a reduced area of lung fibrosis as
227 examined by histology (**Figure 4C, D-E**). Supporting this notion, environmentally adapted mice also showed a
228 lower score of disease burden and a decreased loss of bodyweight during lung fibrosis (**Figure S3C, D**).
229 Furthermore, molecular effectors associated to fibrosis resolution, such as IL-4 and IL-33 were enhanced early
230 after bleomycin inoculation (day 3), whereas profibrotic TSLP (day 14) was decreased during the fibrotic phase
231 in environmentally adapted mice (**Figure S3E-G**). Collectively these functional data reveal a profound
232 regulatory role of environmental adaption for the regulation and severity of acute and chronic inflammation,
233 likely regulated by ApoE⁺CD11b⁺ AMs.

234

235 *Generation of ApoE⁺CD11b⁺ AMs by β-glucan is dependent on the Dectin-1 – Card9 signalling axis.*

236 β-glucan is recognized by various receptors, including CR3, Dectin-1 and CD5 (Fesel and Zuccaro, 2016; Kalia
237 et al., 2021; Taylor et al., 2007). The most prominently expressed receptor on mononuclear phagocytes is
238 Dectin-1. To further understand how development of ApoE⁺CD11b⁺ AMs is regulated on the molecular level,
239 we profiled expression of Dectin-1 on BALF-resident macrophages using flow cytometry (**Figure 5A**). This
240 revealed that homeostatic Dectin-1 expression is largely confined to the resident AM compartment with only a
241 small fraction of monocytes expressing Dectin-1. Further to assess whether expression of Dectin-1 is necessary
242 for the development of ApoE⁺CD11b⁺ AMs, we intranasally inoculated either control or Dectin1^{-/-} mice with β-
243 glucan and analysed the cellular composition of BALF resident immune cells seven days later using flow
244 cytometry. This analysis revealed that generation of ApoE⁺CD11b⁺ AMs is dependent on Dectin-1 expression,
245 whereas initial inflammatory recruitment of Ly6c⁺ monocytes to the air-exposed space is not (**Figure 5B, C**).
246 Next, to understand whether immune cell-intrinsic or stromal cell recognition via Dectin-1 is critical for the
247 development of ApoE⁺CD11b⁺ AMs and thus environmental adaptation, we transferred Dectin1^{-/-} or control
248 (CD45.2⁺) bone marrow into lethally irradiated CD45.1⁺ control mice and analysed their BALF compartment
249 seven days post environmental adaption by β-glucan. Here, generation of ApoE⁺CD11b⁺ AMs was entirely
250 dependent on hematopoietic expression of Dectin-1 (**Figure 5D**). CARD9 has been shown to be a critical
251 molecule for Dectin-1-mediated Nfk β activation (Deerhake et al., 2021; Gross *et al.*, 2006; Vornholz and
252 Ruland, 2020). To investigate whether or not ApoE⁺CD11b⁺ AMs require Card9 for Dectin-1 signalling in order

253 to develop, we treated lethally irradiated mice reconstituted with $\text{Card9}^{-/-}$ or control BM with β -glucan or
254 solvent and analysed the BALF seven days later by flow cytometry. This revealed that development of
255 $\text{ApoE}^+ \text{CD11b}^+$ AMs depends on Dectin-1-elicited Card9 -dependent signalling pathways (**Figure 5E**). Next, we
256 investigated whether the loss of $\text{ApoE}^+ \text{CD11b}^+$ AMs by abrogating Dectin-1 or Card9 signalling also leads to a
257 loss of increased IL-6 secretion upon *in vitro* restimulation with LPS in adherence-selected macrophages. In line
258 with the data obtained in the $\text{CCR2}^{-/-}$ mouse model, enhanced IL-6 secretion was abolished in the absence of
259 Dectin-1 or Card9 signalling and thus can be attributed to $\text{ApoE}^+ \text{CD11b}^+$ AMs (**Figure 5F, G**).
260

261 *Paracrine myeloid-derived Apolipoprotein E controls $\text{ApoE}^+ \text{CD11b}^+$ AM differentiation upon β -glucan-induced*
262 *environmental adaptation.*

263 *Apoe* is highly expressed across a range of monocyte-derived macrophage populations identified in various
264 different low grade or chronic inflammatory diseases, however its exact role in the monocyte to macrophage
265 differentiation and maintenance has not been studied (Aegerter et al., 2020; Jaitin et al., 2019). Similarly, in our
266 model of β -glucan-induced environmental adaptation, *Apoe* was abundantly expressed in CD11b^+ AMs and was
267 also readily detectable on the protein level as early as one day post intranasal β -glucan stimulation within the
268 BALF (**Figure 6A, B**). To further clarify the role of *Apoe* for environmental adaptation of the mononuclear
269 phagocyte repertoire in the lung, we intranasally inoculated $\text{Apoe}^{\text{fl}} \text{Lysm}^{\text{cre}}$ mice with β -glucan, which
270 specifically lack *Apoe* expression within the myeloid lineage, and analysed the composition of the BALF-
271 resident mononuclear phagocyte compartment seven days later using flow cytometry. Here, β -glucan stimulated
272 $\text{Apoe}^{\text{fl}} \text{Lysm}^{\text{cre}}$ mice failed to generate CD11b^+ AMs and in line with this did not have increased numbers of
273 Ly6c^+ monocytes within their BALF (**Figure 6C, D**). Next, we wondered whether *Apoe* was controlling the
274 generation of $\text{ApoE}^+ \text{CD11b}^+$ AMs in a paracrine or autocrine manner as both signalling modes have been
275 described before (Dove et al., 2005; Kemp et al., 2021). Therefore we generated mixed (50:50) wildtype
276 (CD45.1^+) : $\text{Apoe}^{\text{fl}} \text{Lysm}^{\text{cre}}$ (CD45.2^+) bone marrow chimeras or congenic mixed wildtype (CD45.1^+) :
277 wildtype (CD45.2^+) control chimeras. After reconstitution, chimeras were stimulated intranasally with β -glucan
278 and their BALF-resident mononuclear phagocyte repertoire was analysed using flow cytometry seven days later.
279 This analysis revealed that both WT/WT and WT/ $\text{Apoe}^{\text{fl}} \text{Lysm}^{\text{cre}}$ chimeras efficiently generated $\text{ApoE}^+ \text{CD11b}^+$
280 AMs seven days post β -glucan exposure supporting a paracrine signalling mode (**Figure 6E, S4A**). Next, we
281 assessed the contribution of *Apoe*-deficient CD45.2^+ cells to the pool of $\text{ApoE}^+ \text{CD11b}^+$ AMs. This revealed that
282 both *Apoe*-proficient (CD45.1) and deficient (CD45.2) cells equally contributed to the pool of $\text{ApoE}^+ \text{CD11b}^+$

283 AMs post β -glucan stimulation (**Figure 6F**). These data reveal that a paracrine myeloid cell derived source of
284 ApoE is sufficient to rescue the generation of ApoE $^+$ CD11b $^+$ AMs upon environmental adaptation in the lung.

285

286 *Myeloid-derived Apolipoprotein E controls survival of ApoE $^+$ CD11b $^+$ AMs by regulation of cholesterol storage
287 and M-CSF secretion*

288 To reveal the potential mechanism of action for ApoE in the differentiation process of ApoE $^+$ CD11b $^+$ AMs, we
289 investigated whether myeloid-derived ApoE is crucial for the initial commitment of Ly6c $^+$ monocytes towards
290 monocyte-derived macrophage development or if maintenance or survival of monocyte-derived macrophages is
291 controlled by ApoE. To study this, we analysed wildtype or ApoE flox Lysm cre mice three days post intranasal
292 inoculation with β -glucan. Here, ApoE $^+$ CD11b $^+$ AMs and Ly6c $^+$ monocyte numbers within the BALF were
293 comparable between control and ApoE flox Lysm cre mice indicating that initial commitment towards the
294 macrophage lineage and recruitment of monocytic precursors to air-exposed space is not controlled by ApoE,
295 but establishing a critical time window of action for ApoE between day three and day seven post β -glucan
296 inoculation (**Figure 7A, B**). To determine whether ApoE regulates survival of ApoE $^+$ CD11b $^+$ AMs and thus
297 their subsequent longevity *in vivo*, we assessed ApoE $^+$ CD11b $^+$ AM survival three days post β -glucan challenge
298 using TUNEL staining. This analysis showed increased abundance of TUNEL $^+$ ApoE $^+$ CD11b $^+$ AMs in the
299 absence of myeloid derived ApoE upon β -glucan challenge indicating a possible role of ApoE in the regulation
300 of ApoE $^+$ CD11b $^+$ AM survival (**Figure 7C**). To further reveal the possible molecular dysregulation caused by
301 the lack of ApoE in myeloid cells, we evaluated intracellular cholesterol content of BALF resident CD11b $^+$
302 AMs three days post β -glucan stimulation. This revealed that upon β -glucan stimulation ApoE-deficient
303 CD11b $^+$ AMs showed an increase in intracellular cholesterol content as indicated by filipin staining (**Figure 7D,**
304 **E**). Increased intracellular cholesterol storage has been associated to cholesterol induced toxicity by
305 dysregulation of intracellular protein transport (Song et al., 2021). Furthermore, it was shown that autocrine
306 production of M-CSF is crucial for the BALF-resident survival of CD11b $^+$ AMs upon viral infection (Wu et al.,
307 2015). To investigate whether dysregulated M-CSF production due to cholesterol accumulation is involved, we
308 quantified the amount of M-CSF within the BALF of mice intranasally stimulated with β -glucan for 24h. These
309 data showed production of M-CSF within the BALF 24h post β -glucan stimulation in dependence of intact
310 myeloid cell derived ApoE signalling (**Figure 7F, S5A**). Furthermore, fluorescent microscopy revealed that the
311 majority of M-CSF $^+$ cells within the lung also expressed Siglec F and CD11b (**Figure S5B, C**). To understand
312 whether the observed decrease of soluble M-CSF can be attributed to ApoE $^+$ CD11b $^+$ AMs we isolated BALF-

313 resident macrophages by adherence from either control or ApoE^{fl}oxLysm^{cre} mice and assessed the production of
314 M-CSF by CD11b⁺ AMs by microscopy (**Figure 7G**). This showed that ApoE-proficient CD11b⁺ AMs
315 produced increased amounts of M-CSF 24h after β -glucan stimulation whereas ApoE-deficient CD11b⁺ AMs
316 lost their ability to produce M-CSF in response to β -glucan stimulation. Taken together this suggests ApoE as a
317 central regulator of monocyte to macrophage differentiation and survival via the M-CSF signalling axis within
318 the lung upon β -glucan-induced environmental adaptation.

319

320 **Discussion**

321 Within our modern-day environment, the lung is constantly exposed to a plethora of sterile immunostimulatory
322 components. However, the immunological and molecular consequences for lung-resident macrophage
323 development and function are incompletely understood. Here, we show that a single non-pathologic intranasal
324 β -glucan stimulus induces the development of monocyte-derived alveolar macrophages, which highly express
325 CD11b and ApoE and are further characterised by their superior IL-6 production capacity in response to
326 secondary LPS stimulation. Additionally, CD11b⁺ApoE⁺ AMs are glycolytic and modify the outcome of a
327 secondary bacterial infection and of a chronic fibrotic response *in vivo*. Molecularly this adaptation is instructed
328 via the recognition of β -glucan by Dectin-1 and signal transduction via its adaptor protein CARD9. Further
329 examination of the molecular requirements of macrophage adaptation revealed a crucial role of ApoE for
330 maintenance of CD11b⁺ApoE⁺ AMs within the broncho-alveolar environment via the control of macrophage-
331 derived M-CSF. These data reveal that ApoE is a crucial determinant for environmental macrophage adaptation
332 and couples cellular cholesterol metabolism to cellular environmental adaptation.

333 Earlier studies have examined the development of monocyte-derived AMs during pathological insults, such as
334 viral infections, radiation or bleomycin-induced fibrosis (Aegerter *et al.*, 2020; Li *et al.*, 2022a; Machiels *et al.*,
335 2017; Misharin *et al.*, 2017). However, how broncho-alveolar macrophages adapt their transcriptome,
336 metabolism and function to ambient immune stimulatory components, such as LPS or β -glucan, after the acute
337 or sub-acute recognition phase remains poorly understood (Zahalka *et al.*, 2022). Here, we show that although
338 the initial inflammation evoked by β -glucan is minimal, functionally modified monocyte-derived AMs arise
339 from Ly6c⁺ monocytes within the air-exposed space of the lung, a process affiliated to strong pathology-
340 induction, as e.g. found during viral infection. This validates the model as a suitable for low grade
341 environmentally induced inflammation. CD11b⁺ApoE⁺ AMs are induced for up to 21 days post β -glucan
342 stimulation leading to functional modification of the macrophage repertoire in the lung, demonstrating the
343 importance of low-grade inflammatory sterile insults in shaping the overall immune competence of the lung-
344 resident macrophage repertoire.

345 β -glucan is an integral cell wall component of many pathological and non-pathological fungi and can be found
346 within ambient air (Rathnayake *et al.*, 2017). Recent studies evaluated the role of β -glucan for the induction of
347 innate immune training on the systemic level but failed to examine its effects at the level of the tissues exposed
348 (Novakovic *et al.*, 2016; Quintin *et al.*, 2012). Here, β -glucan-induced functional modulations were
349 accompanied by the induction of glycolysis and the enhanced release of the pro-inflammatory cytokines IL-6

350 and TNF α in circulating Ly6 $^+$ monocytes. These findings are in line with our results of the β -glucan-induced
351 functional adaptation in the lung. Furthermore, systemic β -glucan administration was reported to modify bone
352 marrow myeloid development, by expansion of specific GMP / MPP like progenitors, leading to outcomes
353 ranging from enhance pathogen clearance to maladaptation (Kalafati *et al.*, 2020; Li *et al.*, 2022b; Mitroulis *et*
354 *al.*, 2018). In line with these findings, we show that topical subclinical stimulation of the lung with β -glucan
355 only minimally affects bone marrow resident progenitors and that generation of CD11b $^+$ ApoE $^+$ AMs only
356 depends on late stage direct monocytic progenitors and recruitment of Ly6c $^+$ monocytes to the lung via CCR2-
357 dependent signalling. Dectin-1 is crucial for the induction of inflammation upon β -glucan challenge, however
358 its downstream signalling is heterogenous and determines the functional output. We show that tissue adaptation
359 conveys Dectin-1 signalling via CARD9-dependent signalling circuits, in concordance with increased levels of
360 IL-6, most probably via activation of Nfk β signalling.

361

362 Finally, we show that β -glucan-induced macrophages upregulate ApoE, a protein which has been demonstrated
363 to be part of various disease-specific monocyte-derived macrophage gene signatures, e.g. during influenza
364 infection, lung fibrosis or obesity (Aegerter *et al.*, 2020; Jaitin *et al.*, 2019; Misharin *et al.*, 2017). However, its
365 functional role for monocyte-derived macrophage development was not investigated. In hematopoietic stem
366 cells ApoE was shown to inhibit proliferation and subsequent progenitor maturation by controlling sensitivity
367 towards granulocyte macrophage stimulating factor and IL-3 (Murphy *et al.*, 2011). We show that myeloid-
368 specific deletion of ApoE leads to accumulation of intracellular cholesterol, increased cell death and a reduction
369 of autocrine M-CSF production ultimately inhibiting the formation of a long-lived monocyte-derived
370 macrophage compartment upon intranasal β -glucan challenge. Generation of ApoE $^+$ macrophages can also be
371 found in white adipose tissues during obesity, a condition conferring training-like feature to mononuclear
372 phagocytes or during influenza-induced lung inflammation supporting the crucial role of ApoE for the
373 development of functionally adapted macrophages during inflammation (Christ *et al.*, 2018; Jaitin *et al.*, 2019).
374 Other work has established functional Nfk β -responsive elements within the ApoE reporter and CARD9 directly
375 activates Nfk β thus directly couples activation of the inflammatory Nfk β response to the induction of
376 inflammation experience in monocyte-derived macrophages.

377

378 Collectively we provide evidence that a single non-pathological environmental stimulation via the Dectin-1 –
379 CARD9 axis generates inflammation-experienced monocyte-derived macrophages, which modify subsequent

380 acute and chronic inflammation within the lung microenvironment under the control of ApoE, thus molecularly
381 linking macrophage inflammatory amplitude to lung resilience and disease susceptibility.

382 **Acknowledgments**

383 We thank the whole Schlitzer Lab for their fruitful discussion. This study was funded by the Deutsche
384 Forschungsgemeinschaft (DFG, German Research Foundation) under Germany's Excellence Strategy –
385 EXC2151 – 390873048 (AS), and an Emmy Noether research grant (SCHL2116/1 to AS). This research was
386 funded in part by Wellcome Trust [Grant number 217163 and 102705]. For the purpose of open access, the
387 author has applied a CC BY public copyright licence to any Author Accepted Manuscript version arising from
388 this submission. We also thank the Medical Research Council Centre for Medical Mycology at the University of
389 Exeter for funding (MR/N006364/2). M.G. and X.X. were funded by the Swiss National Science Foundation
390 (310030_184915). JLS is supported by the German Research foundation (DFG) under Germany's Excellence
391 Strategy (EXC2151-390873048) as well as under SCHU 950/8-1; GRK 2168, TP11; SFB704, the BMBF-
392 funded excellence project Diet–Body–Brain (DietBB) and the EU project SYSCID under grant SFB 841number
393 733100.

394

395 **Methods**

396 **Animal studies and mouse models**

397 All mice used in this study were bred in the animal facility of the LIMES Institute, University of Bonn,
398 Germany or Center for Translational Cancer Research, Klinikum rechts der Isar, Technical University of
399 Munich, Germany. Animals were housed in IVC mice cages under conventional conditions (12 h/12 h light/dark
400 cycle, 22°C), with ad libitum access to food and water. Eight to twelve weeks old male mice were used for
401 experiments. The ApoE^{fl/fl} mice were kindly provided by Prof. J. Heeren. All experiments were approved by
402 government of North Rhine-Westphalia (84-02.04.2017.A347, 81-02.04.2020.A454).

403

404 **Intranasal stimulation**

405 Mice were anesthetized by intraperitoneal injection of ketamine/xylazine and intranasally inoculated with
406 endotoxin-free 1x PBS (EMD Millipore) or 200 µg β-glucan (\geq 95% pure) from *Candida albicans*, which was
407 provided by Prof. D. Williams. The broncho-alveolar lavage fluid (BALF) was collected one, three, seven, 14 or
408 21 days after inoculation. For cell analysis, the lung was flushed 3x with 1 ml cold 1x PBS with 10 mM EDTA.
409 Afterwards, the fluid was centrifuged for 5 min at 1350 rpm at 4°C and the supernatant was discarded. For
410 cytokine and chemokine assessment, the lung was flushed 3x with the same 1 ml of cold 1x PBS with 10 mM
411 EDTA. Afterwards, the samples were centrifuged for 10 min at 14000 rpm at 4°C and the supernatant was

412 frozen in liquid nitrogen until analysis. Supernatants were thawed on ice and centrifuged for 5 min at 10 000 rpm
413 at 4°C to remove debris. M-CSF (R&D Systems) and ApoE (Abcam) protein levels were measured by ELISA
414 according to manufacturer's protocols.

415

416 **Pulmonary fibrosis and *Legionella pneumophila* infection**

417 Mice were intranasally stimulated with β -glucan or PBS seven days before induction of pulmonary fibrosis or
418 infection by *Legionella pneumophila*. For fibrosis induction, *Streptomyces verticillus* bleomycin (Sigma-
419 Aldrich, 0.75 mg/kg body weight) was administered by intratracheal gavage. Body weight and health status
420 were scored on a daily basis. Analysis was performed three or 14 days after bleomycin application. For bacterial
421 infections, intratracheal application of *Legionella pneumophila* (5×10^6 CFU/mouse) was performed and mice
422 were sacrificed 2 days after induction. *L. pneumophila* was provided by A. Oxenius. Bacteria from the glycerol
423 (25%) stock were plated on a CYE-plate and grown for 3 days at 37°C in a non-CO₂ incubator. For bacterial
424 load determination one lobe of the lung was collected in 1 mL PBS with 1 metal bead and smashed using a
425 tissue lyser (Qiagen). 25 μ L of lysed lung were put in duplicates on CYE-plates and grown for 3-4 days at 37°C
426 in a non-CO₂ incubator.

427

428 **Bone marrow Chimeras**

429 Bone marrow chimeras were generated by multiple intraperitoneal busulfan (Sigma-Aldrich) injections or
430 irradiation of recipient mice with 10 Gy. Afterwards, 5×10^6 (busulfan-treated mice) or 1.5×10^6 (irradiated
431 mice) freshly isolated bone marrow cells from the donor animals were intravenously injected into the recipients.
432 Peripheral blood chimerism was assessed 28 days after reconstitution by flow cytometry. Bone marrow
433 chimeras were used in experiments after eight – twelve weeks of reconstitution.

434

435 **Flow cytometry and cell sorting**

436 For flow cytometry, cells of the broncho-alveolar space were harvested by flushing the lungs with 3x 1 ml ice
437 cold 1x PBS containing 10 mM EDTA. After centrifugation with 1350 rpm for 5 min at 4°C, cell pellets were
438 resuspended in antibody mix and stained for 35 min at 4°C. After washing with FACS buffer (1x PBS, 2 mM
439 EDTA, 0.5% BSA (SERVA)), life/death stain was performed using DRAQ7 (BioLegend, 1:1000 in FACS
440 buffer) for 5 min at RT. Red blood cell lysis was performed only if necessary. In case of blood analysis, blood
441 was collected in 1x PBS with 10 mM EDTA and stained in antibody mix for 35 min at 4°C. Red blood cell lysis

442 was performed twice for 5 min at RT before life/death stain and acquisition. For bone marrow cells, femur and
443 tibia were flushed with 1x PBS, stained with antibody mix for 1 h and red blood cell lysis and life/death stain
444 were subsequently performed. Cells were washed and resuspended in FACS buffer and recorded using FACS
445 Symphony A5 (Becton Dickinson). FACS data were analyzed using FlowJo v10.8.1 (Becton Dickinson).
446 Cell sorting was performed using an ARIA III (Becton Dickinson) instrument. Briefly, cells from the lung
447 lavage were antibody stained followed by life/death stain. Cell sorting was performed using a 100 μ m nozzle
448 into cooled 1.5 ml reaction tubes containing FACS buffer.

449

450 ***Ex vivo* stimulation and assessment of cytokine production**

451 BALF of stimulated mice was collected in 15 ml tubes, centrifuged at 1350 rpm for 5 min at 4°C and
452 resuspended in 1 ml RPMI1640 (PAN Biotech) supplemented with 10% FCS (Sigma-Aldrich), 2 mM
453 GlutaMAX (Gibco), 5 ml MEM non-essential amino acids (Sigma Aldrich), 1 mM Na-Pyruvate (Gibco), 50
454 U/ml Pen-Strep (Gibco) and 500 μ l β -Mercaptoethanol. Cells were counted and seeded with 0.2 $\times 10^5$ cells per
455 well. After 2 h resting in 500 μ l medium at 37°C and 5% CO₂, cells were stimulated with 10 ng/ml LPS (Sigma-
456 Aldrich). After 24 h, cell culture supernatant was harvested and snap frozen for further analysis. Supernatants
457 were thawed on ice and centrifuged for 5 min at 10 000 rpm at 4°C to remove debris. TNF- α and IL-6
458 (ThermoFisher) protein levels were measured by ELISA. For multiplex cytokine and chemokine analysis, a
459 customized 18-plex Procartaplex kit (ThermoFisher) was used according to manufacturer's protocols and run on
460 Luminex FLEXMAP 3D (ThermoFisher) device.

461

462 **Intracellular cytokine stain**

463 Lavage fluid of two mice was pooled and centrifuged for 5 min at 1350 rpm at 4°C. Cells were resuspended in 1
464 ml RPMI1640 (PAN Biotech) supplemented with 10% FCS (Sigma-Aldrich), 2 mM GlutaMAX (Gibco), 5 ml
465 MEM non-essential amino acids (Sigma Aldrich), 1 mM Na-Pyruvate (Gibco), 50 U/ml Pen-Strep (Gibco) and
466 500 μ l β -Mercaptoethanol. Equal cell numbers were plated into two wells per condition and rested in 500 μ l
467 media for 2 h at 37°C and 5% CO₂. Cells were stimulated with 10 ng/ml LPS (Sigma-Aldrich) for 6 h in total.
468 After 4 h, 2.5 μ g Brefeldin A (BioLegend) and 2 nM Monensin (BioLegend) were added to each well and
469 incubated for further 2 h. Afterwards, supernatant was discarded and cells were harvested in 1xPBS using a cell
470 scraper followed by staining of surface markers by antibodies for 30 min at 4°C. Cells were washed and
471 permeabilized using the Cytofix/Cytoperm kit (Becton Dickinson, adapted from manufacturer's protocol). In

472 brief, cells were resuspended in 200 μ l Cytofix/Cytoperm solution per tube and incubated for 20 min at 4°C.
473 Cells were washed twice with Perm/Wash and stained with Zombie NIR fixable viability dye (1:1000 in PBS)
474 for 15 min. After washing with Perm/Wash, cells were intracellularly stained by 100 μ l Perm/Wash containing
475 IL-6 (MP5-20F3; 1:100) or TNF- α (MP6-XT22; 1:100) antibody or the corresponding isotype control for 30
476 min at 4°C. Cells were washed twice with Perm/Wash and resuspended in 1x PBS before acquisition.

477

478 **Seahorse analysis**

479 BAL fluid of two mice was pooled and 50.000 – 100.000 cells were plated in a 96 well Seahorse plate (Agilent)
480 in Seahorse XF base medium (Agilent) supplemented with 5% L-Glutamine (Sigma-Aldrich), 10% FCS
481 (Sigma-Aldrich) and 50 U/ml Pen/Strep (Gibco) for 2 h at 37°C and 5% CO₂. Before acquisition, cells were
482 washed and incubated in Seahorse XF base medium with 5% L-Glutamine (Sigma-Aldrich) and 50 U/ml
483 Pen/Strep (Gibco), but without FCS and Glucose for 30 min at 37°C without CO₂ supply. During the Seahorse
484 run, 100 mM Glucose (Sigma-Aldrich) solution was injected into port A leading to a final glucose concentration
485 of 10 mM per well. This was followed by injection of 10 μ M Oligomycin A (Sigma-Aldrich, final concentration
486 1 μ M) solution and 500 mM 2-Desoxyglucose (Sigma-Aldrich, final concentration 50 mM). Glycolysis,
487 glycolytic capacity and glycolytic reserve were calculated using the Agilent Wave software.
488 After the Seahorse assay, cell numbers of each well were determined using the CyQUANT NF Cell
489 Quantification Assay (Thermo-Fisher) for normalization. 50 μ l of CyQUANT NF Cell Quantification mix were
490 added to each well, incubated for 30 min at RT and measured in a TECAN plate reader (excitation wavelength
491 485 nm, emission wavelength 530 nm).

492

493 **Histology**

494 Mice were anesthetized followed by trans-cardial perfusion with 10ml ice cold 1xPBS containing 10 mM EDTA
495 using the lung-heart circulation. Lungs were removed and fixed in 4% PFA overnight at 4°C (for paraffin-
496 embedded tissue) or infiltrated with 1 mL 50% OCT (in 1xPBS), removed, and fixed for 6 h in 1.3% PFA at
497 4°C. For paraffin sections lungs were dehydrated and paraffin embedded. For frozen sections, after fixation
498 lungs were dehydrated in 10, 20, and 30% sucrose (in 1x PBS) for 24 h at 4°C. After dehydration, the left lobe
499 was separated and embedded in OCT. Sections of 5 μ m were prepared for Hematoxylin and Eosin (H&E) and
500 Trichrome (Masson) stainings and immunohistochemistry.

501

502 **Immunofluorescence and histology stainings**

503 Coverslips containing frozen tissue sections were left drying on drierite beads for 5min and subsequently fixed
504 on ice-cold acetone for 10 min. Afterwards, sections were washed twice with 0.01% Tween-PBS and
505 permeabilized with 0.2% Triton X-100 for 20min at RT. After permeabilization, sections were washed twice
506 with 1x PBS and photobleached as described before (Du et al., 2019). Following photobleaching, sections were
507 blocked in 3% BSA (prepared in 1xPBS) for 1 h at RT. After blocking, primary antibodies were diluted in 0.5%
508 BSA, added to the sections, and left incubating overnight at 4°C. Sections were then washed three times with 1x
509 PBS and secondary antibodies (diluted in 0.5% BSA solution containing nuclear staining) were subsequently
510 added and left incubating for 1 h at RT protected from light. Secondary antibodies were washed as before and
511 coverslips were mounted on a glass slide using mounting medium. If using fluorescently labeled primary
512 antibodies, these were added after washing the secondary antibodies and left incubating 2 h at RT. For
513 immunofluorescence of cultured cells no acetone fixation and photobleaching were performed. For Trichrome
514 (Masson) stainings, glass slides containing paraffin-embedded tissue sections were placed on a heating block set
515 to 56°C for 30 min to melt the paraffin. Afterwards, sections were washed twice in xylol (5 min each) and
516 rehydrated in decreasing alcohol concentrations (100%, 100%, 90%, 70%, 50%, 30%), for 3 min each. For
517 Trichrome (Masson) staining, samples were left overnight in Boulin's solution and subsequently stained
518 following manufacturer's instructions. Samples were mounted with a xylol-compatible mounting medium.

519

520 **Filipin and TUNEL stainings**

521 5-8x10⁴ BALF cells were seeded in complete RPMI medium in a 24-well plate containing 10 mm sterile glass
522 coverslips. Cells were left adhering for 3 h at 37°C. For filipin and TUNEL stainings, cells were washed with 1x
523 PBS and subsequently fixed with 4% PFA for 30 min. For filipin staining, after washing away the fixative, cells
524 were incubated in 100 mM glycine for 10 min at RT, and subsequently blocked with 3% BSA supplemented
525 with 50 µg/ml filipin for 2 h at RT. Cells were washed three times with 1x PBS and immunostained as indicated
526 above, but DRAQ5 was used as a counterstain. For TUNEL staining, manufacturer's instructions were followed
527 and immunofluorescence was performed after TUNEL.

528

529 **Imaging**

530 Images of Trichrome stainings were acquired with a Zeiss Axio Observer microscope using a 20x air objective
531 (NA 0.85). Multiple tiles, covering the entire section, with an overlap of 10% were acquired and stitched with

532 the ZEN 3.2 software. Images of immunofluorescence of tissue sections and cultured cells were acquired using a
533 Zeiss LSM 880 Airyscan system using a 60x oil immersion objective (NA) with a z-spacing of 500 nm. Images
534 were acquired using the 405, 488, 561 and 640 nm laser lines. During acquisition, nuclei showing the
535 prototypical shape of neutrophils or eosinophils were excluded.

536

537 **Image analysis**

538 To quantify signal intensities from different markers from individual BALF cells, images were analyzed with a
539 customized pipeline in CellProfiler. Briefly, Hoechst or DRAQ5 signals were used to segment the cells. A
540 second primary detection step was added to create a mask of all SiglecF⁺ objects. This mask was subsequently
541 merged onto the nuclei mask and only overlapping objects were further analyzed. A secondary object detection
542 step was incorporated to distinguish between CD11b⁺ and CD11b⁻ cells and create a mask of alveolar
543 macrophages. In all detection steps clumped objects were separated based on shape and signal intensities. Mean
544 intensities for all channels for every single object were exported and used for analysis. Analysis of
545 immunofluorescence of tissue sections was performed in QuPath. As before, Hoechst signal intensities were
546 used to identify all objects using a radius of 2 μ m. For each channel, an object classifier was created to set the
547 detection threshold based on the mean signal intensity. Subsequently, these classifiers were combined to
548 identify alveolar macrophages. Individual cell mean intensities were exported. To measure the percentage and
549 area of fibrosis, Trichom staining images were imported into QuPath. The total tissue area was manually
550 annotated. A pixel classifier was trained to detect fibrotic and healthy areas. For this purpose, 5 exemplary
551 regions of fibrotic and healthy areas were selected. Area and percentage of fibrosis were the output of this
552 trained pixel classifier. The created classifier was applied in all the sections analyzed.

553

554 **CODEX multiplexed imaging and analysis**

555 5 μ m fresh frozen sections of the left lobe of the lung of 8-week *Ms4a3-cre*^{Rosa26TOMATO} mice stimulated
556 intranasally with PBS or β -glucan for seven days were prepared and stained following manufacturer's
557 instructions. Briefly, sections were retrieved from the freezer, let dry on drierite beads, and fixed in ice-cold
558 acetone for 10 min. Following fixation, samples were rehydrated and permeabilized for 20 min with 0.2%
559 Triton-X100. To reduce tissue autofluorescence, sections were photobleached twice for 1 h as indicated before
560 (Du *et al.*, 2019). After photobleaching, samples were washed, equilibrated for 30 min in staining buffer (Akoya
561 Biosciences, Marlborough, MA, USA), and subsequently stained with a 17-plex CODEX antibody panel

562 overnight at 4°C. After staining, samples were washed in staining buffer, fixed in ice-cold methanol to improve
563 imaging quality and washed. A final fixation step with BS3 crosslinker (Sigma Aldrich) was performed.
564 Specimens were stored in CODEX storage buffer (Akoya Biosciences) at 4°C for a maximum of one week
565 before imaging. Antibody detection was performed in a multicycle experiment with the corresponding
566 fluorescently-labeled reporters, following manufacturer's instructions. Images were acquired with a Zeiss Axio
567 Observer widefield microscope (Carl Zeiss AG, Jena, Germany) using a 20x air objective (NA 0.85) and a z-
568 spacing of 1.5 μm. The 405, 488, 568, 647 nm fluorescent channels were used. After acquisition, images were
569 exported using the CODEX Instrument Manager (CIM, Akoya Biosciences) and processed with the CODEX
570 Processor v1.7 (Akoya Biosciences). Processing steps included background subtraction, stitching, shading
571 correction, deconvolution, and cell segmentation. Cells were segmented using DAPI signals and ATPase I
572 membrane staining to define the cell borders. Cell classification to detect alveolar macrophages and other
573 mononuclear phagocytes was performed in CODEX MAV (Akoya Biosciences), following a similar gating
574 scheme as the one used for flow cytometry.

575

576 **Preparation of Seq-Well arrays**

577 Seq-Well arrays were prepared as previously described (Gierahn et al., 2017). Briefly, PDMS master mix
578 (sylgard base, crosslinker, 10:1 ratio) was poured into a master mold and incubated for 2 h at 70°C to generate
579 the arrays. Afterwards, the arrays were functionalized and rinsed with 100% EtOH, dried at RT and plasma
580 treated for 7 min. After submerging in APTES and PDITC buffers, the arrays were washed in acetone and dried
581 for 2 h at 70°C followed by incubation in 0.2% chitosan solution (pH=6.3) at 37°C for 1.5 h. After chitosan
582 incubation, the arrays were incubated overnight in PGA buffer at RT under vacuum pressure and rotated for 3 h.

583

584 **Preparation of Seq-Well libraries**

585 Seq-Well libraries were generated as previously described (Gierahn et al., 2017). Briefly, 110000 barcoded
586 mRNA-capture beads in Bead Loading Buffer were loaded onto the array. Afterwards, the Bead Loading Buffer
587 was replaced by RPMI 1640 medium (Gibco) with 10% FCS (Sigma-Aldrich) and incubated for 10 min. The
588 medium was discarded, 20000 to 30000 BALF cells were loaded and rocked for 10 min. The loaded arrays were
589 washed 5x with PBS, soaked in RPMI 1640 and sealed by polycarbonate membranes under mild vacuum. The
590 sealed arrays were incubated for 37°C for 30 min in Agilent clamps (Agilent) and then incubated in a
591 guanidinium-based lysis buffer for 20 min. After incubation in hybridization buffer, the mRNA capture beads

592 were washed from arrays and collected. Reverse transcription was performed on the bead pellet using a Maxima
593 Reverse Transcriptase reaction (ThermoFisher) for 30 min at room temperature with end-over-end rotation
594 followed by 90 min incubation at 52°C with end-over-end rotation. The reaction was stopped by washing with
595 TE buffer supplemented with 0.01% Tween-20 or 0.5% SDS. Excess primers were digested by exonuclease
596 ExoI (New England Biolabs). Beads were counted and the reverse transcribed cDNA libraries were amplified in
597 a PCR reaction. After PCR, 20000 – 40000 beads were pooled and cleaned using AMPure XP beads (Beckman
598 Coulter). The library integrity was assessed using a High Sensitivity D5000 assay (Agilent) for Tapestation
599 4200 (Agilent).

600

601 **Sequencing**

602 Tn5 was mixed with pre-annealed linker oligonucleotides and supplemented with glycerol, dialysis buffer and
603 H₂O. The cDNA libraries (1 ng) were tagmented with the prepared single-loaded Tn5 transposase and
604 afterwards cleaned using MinElute PCR kit (Qiagen) following the manufacturer's instructions. The Illumina
605 indices (Illumina) were added to the tagmented product by PCR, which was subsequently cleaned with AMPure
606 XP beads (Beckman Coulter). The final library quality was assessed using a High Sensitivity DNA5000 assay
607 (Agilent) and quantified using the Qubit high-sensitivity dsDNA assay (ThermoFisher). Seq-Well libraries were
608 equimolarly pooled and clustered at 1.4 pM concentration with 10% PhiX using High Output v2.1 chemistry
609 (Illumina) on a NextSeq500 system (Illumina). Sequencing was performed paired-end as followed: custom
610 Drop-Seq Read 1 primer for 21 cycles, 8 cycles for the i7 index and 61 cycles for Read 2. Single-cell data were
611 demultiplexed using bcl2fastq2 (v2.20) (Illumina). Fastq files were loaded into a snakemake-based data pre-
612 processing pipeline (version 0.31, available at <https://github.com/Hoohm/dropSeqPipe>) that relies on the Drop-
613 seq tools provided by the McCarroll lab (Macosko et al., 2015).

614

615 **scRNaseq data analysis**

616 Sequencing reads were mapped to the mouse reference genome mm10 using STAR alignment from the Drop-
617 seq pipeline (v2.0.0) as previously described (Macosko, Cell, 2015). Next, we assess the quality of our libraries
618 and excluded cells with low quality (<500 genes per cell), doublets (>3000 genes per cell), or dead cells (>10%
619 of mitochondrial content). All genes expressed in less than 5 cells were filtered out.

620 Cell clustering analysis was performed using the Seurat package (v4.1.1) according to instructions (Hao et al.,
621 2021). In brief, the expression data was log normalized with a scale factor of 10.000. After scaling, PCA was

622 performed using the top 3000 variable genes for a linear dimensional reduction. The first 15 PCA components
623 were used to cluster cells by the Louvain algorithm. To obtain an optimal cluster resolution, we set the
624 resolution parameter in the FindClusters function as 0.25 to generate 5 major clusters, which were visualized
625 after non-linear dimensional reduction with UMAP. Differentially expressed genes (DEGs) in each cluster were
626 identified by using the default Wilcoxon rank sum test in the FindAllMarkers function, and were defined with
627 logfc.threshold >0.25 and min.pct >0.25.

628

629 **Code and Data availability**

630 The scRNA-seq raw reads and processed data were submitted to the NCBI GEO database accession number
631 GSE211575. All code used for data visualization of the scRNA-seq data can be found at
632 https://github.com/JiangyanYu/Trained_Immunity_2022.

633

634 **Statistics**

635 Statistical analysis and comparison was performed using Prism 9 (GraphPad). Data are shown as mean \pm SD.
636 Statistical significance was assessed by student's *t*-test (unpaired) or ordinary one-way ANOVA with Tukey's
637 multiple comparisons test. Survival of animals is displayed in Kaplan-Meier survival curves. A p value < 0.05
638 was considered as statistically significant (* P < 0.05, ** P < 0.01, *** P < 0.001, **** P < 0.0001). Mice were
639 randomly allocated to the control or treatment groups by the investigator. Mice numbers are indicated as "n" in
640 the figure legends.

641

642 **Author contributions**

643 Conceptualization: H.T., D.A.B., J.H., N.K., A.S.; Formal Analysis and Investigation: H.T., D.A.B., J.H., N.K.,
644 J.S-S., K.B., J.Y., C.O.S., F.P., M.K., L.V., Y.X., M.G., L.B., A.A., S.C., K.H., G.B., D.L.W., F.G., J.R., M.B.,
645 J.L.S.; Writing:H.T., D.A.B., J.H., A.S.; Supervision:A.S..

646

647 **Figure Legends**

648 **Figure 1 Intranasal β -glucan exposure generates environmentally adapted ApoE⁺CD11b⁺ alveolar
649 macrophages within the broncho-alveolar space.**

650 (A-E) Single-cell RNA sequencing of the broncho-alveolar lavage fluid (BALF) of male 8-12 weeks old
651 C57BL/6JCrI mice after intranasal stimulation with 40 μ l 200 μ g β -glucan or PBS (n=10202 cells). Seven days
652 after exposure, cells were harvested and sorted for SSC^{hi}, Lin⁻ (B220, CD19, CD3 ϵ , Nk1.1, Ter-119), DRAQ7⁻
653 singlets. (A) Uniform-manifold approximation and projection (UMAP) analysis of both conditions combined
654 shows five different clusters. (B) Heatmap of top ten highly expressed genes for each of the five clusters. (C, D)
655 UMAP from (A) separated by PBS (C, n= 4845 cells) or β -glucan (D, n= 5357 cells) condition. (E) Percentage
656 of contribution of the five annotated clusters to overall cells split by conditions. (F) 5 μ m frozen section of the
657 left lobe of the lung of a *Ms4a3-cre*^{Rosa26TOMATO} mouse 7 days after β -glucan exposure stained with a 17-plex
658 CODEX antibody panel. Overlay image shows the markers used to identify AM populations. Single stainings of
659 these markers are shown in grayscale. Arrows indicate CD11b⁺ ApoE⁺ AMs. Scale bar represents 100 μ m. (G)
660 Flow cytometric quantification of absolute ApoE⁺CD11b⁺ AM (CD45⁺SiglecF⁺CD64⁺CD11c⁺CD11b⁺)
661 numbers in the BALF in a time course from 1 to 21 days post β -glucan stimulation of wt mice (n= 5).

662

663 **Figure 2 ApoE⁺CD11b⁺ AMs are monocyte-derived and CCR2-dependent.**

664 (A) Flow cytometric quantification of absolute Ly6c⁺ monocyte (CD45⁺Ly6g⁻SiglecF⁺CD64⁺CD11b⁺Ly6c⁺)
665 numbers in the BALF 1 to 21 days post β -glucan stimulation of C57BL/6J mice (n=4-5). (B, C) Flow cytometric
666 analysis of BALF from *Ms4a3-cre*^{Rosa26TOMATO} mice seven days after intranasal PBS or β -glucan stimulation
667 (n=3). (B) Percentage of Tomato⁺ labelling in CD11b⁻ and CD11b⁺ AM and (C) proportion of Tomato⁺ labelling
668 in CD11b⁻ and CD11b⁺ AM compared to monocytes (CD45⁺SiglecFLy6g⁻CD11b⁺F4/80⁺). (D) CODEX
669 multiplexed immunostaining of the left lobe of a *Ms4a3-cre*^{Rosa26TOMATO} mouse 7 days after β -glucan exposure
670 (enlargement from Fig. 1F). Filled arrowheads indicate CD11b⁺ ApoE⁺ AMs, whereas empty arrowheads
671 indicate CD11b AMs. dtTomato reporter signals are represented in red. Scale bar represents 50 μ m. (E) Flow
672 cytometric quantification of absolute CD11b⁺ AM numbers in the BALF seven days after β -glucan exposure in
673 wt or CCR2^{-/-} mice (n=8). (F-K) Percentage and absolute counts of Ly6c⁺ monocytes in the blood (F, G, n=12)
674 or Ly6c⁺ monocytes and MHCII⁺ cMOPs in the bone marrow (H-K, n=4) of C57BL/6J mice seven days after
675 PBS or β -glucan by flow cytometry. (K) Flow cytometric quantification of GMPs in the bone marrow of
676 C57BL/6J mice three days after intranasal PBS or β -glucan stimulation by flow cytometry (n = 8).

677

678 **Figure 3 ApoE⁺CD11b⁺ AMs show increased release of interleukin 6 and induction of glycolysis.**

679 (A-C) BALF cells were harvested from C57BL/6J mice seven days after intranasal exposure with PBS or β -
680 glucan and subsequently restimulated *in vitro* with PBS or LPS. (A) Quantification of IL-6 protein levels by
681 ELISA in the cell culture supernatant 24 h after LPS restimulation (n=15). (B) Intracellular staining and flow
682 cytometric measurement of IL-6. Dot plot shows the percentage of IL-6⁺ CD11b⁺ AM after restimulation with
683 LPS for 6-8 h followed by intracellular staining and flow cytometric analysis (n=6). (C) Representative flow
684 cytometry dot plots of (B) gated on CD11b⁺ AM. (D) Quantification of IL-6 protein levels by ELISA in the cell
685 culture supernatant 24 h after restimulation with LPS of C57BL/6J (n=15) and CCR2^{-/-} mice (n=4). (E, F)
686 Extracellular flux analysis acidification rate (E) and glycolysis (F) in BALF cells seven days after PBS or β -
687 glucan stimulation (n=6).

688

689 **Figure 4 β -glucan-induced environmental adaptation enhances pulmonary bacterial clearance and
690 ameliorates bleomycin-induced fibrosis.**

691 (A, B) C57BL/6J mice were intranasally stimulated with PBS or β -glucan followed by intratracheal infection
692 with *Legionella pneumophila* at day seven post primary stimulation and analysis at day nine (n=4).
693 Quantification of bacterial load in BALF (A) and absolute numbers of CD11b⁺ AM by flow cytometry nine
694 days post primary stimulation (B). (C-E) Pulmonary fibrosis was induced seven days after PBS or β -glucan
695 stimulation by intratracheal gavage of *Streptomyces verticillus* bleomycin. (C) Mice were monitored daily for
696 survival (n=14). (D-E) Representative images of Masson's Trichome staining of lung tissue at day 21 after
697 initial stimulation (E) and quantification of fibrotic areas (D). Each dot in (D) represents a mouse. Scale bar in
698 (E) represents 500 μ m.

699

700 **Figure 5 Generation of ApoE⁺CD11b⁺ AMs by β -glucan is dependent on the Dectin-1 – Card9 signalling
701 axis.**

702 (A) Percentage of monocyte and macrophage populations contributing to Dectin-1⁺ cells in the C57BL/6J
703 mouse lung pre gated on CD45⁺Lin⁻Ly6g⁻CD64⁺ cells (n=6) by flow cytometry. (B, C) Absolute CD11b⁺ AM
704 (B) and Ly6c⁺ monocyte (C) numbers in the BALF seven days after PBS or β -glucan exposure in C57BL/6J or
705 Dectin1^{-/-} mice (n=5-9) by flow cytometry. (D, E) Absolute CD11b⁺ AM numbers in the BALF seven days after
706 PBS or β -glucan exposure in Dectin1^{-/-} (D, n=3-6) or Card9^{-/-} (E, n=8-9) bone marrow chimeras by flow

707 cytometry. (F) Quantification of IL-6 protein levels by ELISA in the cell culture supernatant 24 h after LPS
708 restimulation of C57BL/6J (n=15) and Dectin1^{-/-} mice (n=7-8). (G) Quantification of IL-6 protein levels by
709 ELISA in the cell culture supernatant 24 h after LPS restimulation of C57BL/6J (n=3-5) and Card9^{-/-} mice (n=5).
710

711 **Figure 6 Paracrine myeloid-derived Apolipoprotein E controls ApoE⁺CD11b⁺ AM differentiation upon β -
712 glucan-induced environmental adaptation.**

713 (A) Violin plot of *ApoE* RNA expression levels in the BALF seven days after β -glucan exposure by scRNA seq.
714 (B) C57BL/6J mice were stimulated with β -glucan and BALF was harvested at different time points. Plot shows
715 ApoE protein levels in the BALF measured by ELISA (n=5). (C, D) Absolute numbers of CD11b⁺ AM (C) and
716 Ly6c⁺ monocytes (D) seven days after intranasal β -glucan exposure of C57BL/6J or ApoE^{flx}LysM^{cre} mice by
717 flow cytometry (n=8-10). (E, F) Lethally irradiated CD45.1⁺/CD45.2⁺ male mice were reconstituted with
718 1.5x10⁶ CD45.1⁺ mixed with CD45.2⁺ bone marrow cells (WT/WT) or with CD45.1⁺ mixed with
719 ApoE^{flx}LysM^{cre} CD45.2⁺ bone marrow cells (WT/ ApoE^{flx}LysM^{cre}) for 12 weeks and subsequently intranasally
720 stimulated with PBS or β -glucan (n=4-5). Flow cytometric quantification of CD11b⁺ AM numbers (E) and
721 contribution of donor cells (CD45.1⁺ or CD45.2⁺) to the CD11b⁺ AM pool (F) seven days after exposure.
722

723 **Figure 7 Myeloid-derived Apolipoprotein E controls survival of ApoE⁺CD11b⁺ AMs by regulation of
724 cholesterol storage and M-CSF secretion.**

725 (A-B) Absolute numbers of CD11b⁺ AM (A) and Ly6c⁺ monocytes (B) three days after intranasal β -glucan
726 exposure in C57BL/6J or ApoE^{flx}LysM^{cre} mice (n=7-8) by flow cytometry. (C-E) C57BL/6J and
727 ApoE^{flx}LysM^{cre} mice were stimulated with PBS or β -glucan intranasally. Three days after stimulation, BALF
728 was harvested, seeded and fixed after 2 h. (C) TUNEL staining was performed, followed by conventional
729 immunofluorescence to detect SiglecF and CD11b. Plot shows mean TUNEL signal intensities of individual
730 CD11b⁺ AM (n=4). (D, E) Filipin staining after fixation and immunofluorescence analysis. Representative
731 images of filipin stainings are shown in (D). Scale bars represent 5 μ m. Plot in (E) shows mean filipin signal
732 intensities of individual CD11b⁺ AM in the different conditions (n=5). (F) Quantification of M-CSF protein
733 levels in the BALF one day after β -glucan exposure in C57BL/6J mice or ApoE^{flx}LysM^{cre} mice (n=6) measured
734 by ELISA. (G) C57BL/6J and ApoE^{flx}LysM^{cre} mice were stimulated with PBS or β -glucan intranasally. 24 h
735 after stimulation BALF was harvested and seeded. Cells were fixed after 2h and immunostained to detect
736 SiglecF, CD11b, and M-CSF. Plot shows mean M-CSF signal intensities of individual CD11b⁺ AMs (n=4).

737

738 **Supplement Figure 1 to Figure 1**

739 (A-E) Quality control of the scRNA sequencing dataset of the BALF seven days after intranasal stimulation
740 with PBS or β -glucan in wt mice. (A) Violin plot of feature gene counts per cluster. (B) Violin plot of UMI
741 counts per cluster. (C) Violin plot of mitochondrial gene percentage per cluster. (D, E) Violin plot of *SiglecF* (D)
742 and *Itgax* (E) RNA expression levels in the BALF seven days after β -glucan exposure by scRNA seq. (F)
743 Percentage of contribution of condition, PBS or β -glucan, to the five clusters. (G) Flow cytometry gating
744 strategy pre-gated on Lin $^{-}$ (Ly6g, B220, CD19, CD3 ϵ , Nk1.1, Ter-119) and CD45 $^{+}$ cells to define CD11b $^{+}$ AM
745 in the BALF after intranasal PBS or β -glucan stimulation. (H) Flow cytometric quantification of AM
746 (CD45 $^{+}$ SiglecF $^{+}$ CD64 $^{+}$ CD11c $^{+}$) numbers in the BALF in a time course from 1 to 21 days post β -glucan
747 stimulation of wt mice (n= 5). (I) UMAP representation of intranasally stimulated lungs with PBS or β -glucan
748 seven days after stimulation (pooled n=3 per condition). (J) Mean fluorescence Intensity (MFI) of Siglec F on
749 indicated cell subsets in lung seven days post stimulation with β -glucan (n=4).

750

751 **Supplement Figure 2 to Figure 3**

752 (A-C) BALF cells were harvested from wt mice seven days after intranasal exposure with PBS or 40 μ l 200 μ g
753 β -glucan and subsequently restimulated *in vitro* with PBS or 10 ng/ml LPS. (A) Quantification of TNF- α
754 protein levels by ELISA in the cell culture supernatant 24 h after restimulation with LPS (n=15). (B)
755 Intracellular staining and flow cytometric measurement of TNF- α . Plot shows the percentage of TNF- α $^{+}$
756 CD11b $^{+}$ AM after restimulation with LPS for 6-8 h followed by intracellular staining and flow cytometric
757 analysis (n=6). (C) Representative flow cytometry dot plots of (B) gated on CD11b $^{+}$ AM. (D, E) Measurement
758 of glycolytic reserve (E) and glycolytic capacity (F) in BALF cells seven days after PBS or β -glucan stimulation
759 with Seahorse (n=6).

760

761 **Supplement Figure 3 to Figure 4**

762 (A) Experimental setup of β -glucan-induced environmental adaptation followed by an acute infection. Intranasal
763 PBS or β -glucan stimulation at day zero was followed by intratracheal inoculation with *Legionella pneumophila*
764 at day seven and sacrifice two days after infection. (B) Experimental setup of β -glucan-induced environmental
765 adaptation followed by bleomycin-induced lung fibrosis. Intranasal PBS or β -glucan stimulation at day 0 was
766 followed by intratracheal application of *Streptomyces verticillus* bleomycin at day seven and sacrifice three or

767 14 days after fibrosis induction. (C, D) Disease burden and body weight of mice after pretreatment PBS or β -
768 glucan (day 0) prior to fibrosis induction (day seven). To evaluate the disease burden (C), mice were scored for
769 general health appearance, spontaneous behavior and body weight (n=14). (D) Body weight changes were
770 calculated as % change based on the initial weight at day 0 (n=14). (E-G) Quantification of IL-4 (E), IL-33 (F)
771 and TSLP (G) protein levels using Luminex Procartaplex kit 3 or 14 days after bleomycin treatment (n=7 per
772 condition).

773

774 **Supplement Figure 4 to Figure 6**

775 (A) Ly6c⁺ monocyte chimerism of WT/WT or WT/ApoE^{flox}LysM^{cre} chimeras in BALF, blood and BM at the
776 day of sacrifice. Bars are further subdivided to display contribution of transferred mixed bone marrow donors.

777

778 **Supplement Figure 5 to Figure 7**

779 (A) Quantification of M-CSF protein levels in the BALF in a time course from one to 21 days post β -glucan
780 stimulation of C57BL/6J mice (n=5). (B, C) Lungs from C57BL/6J mice were harvested 24 h after β -glucan
781 stimulation, fixed, and frozen in OCT. 5 μ m sections were prepared and stained with antibodies to identify AMs
782 and visualize M-CSF production. Representative images are shown in (B). Arrows indicate CD11b⁺ AMs.
783 Seven regions of the same size from samples in (B) were acquired and analyzed as explained in Materials and
784 Methods. Plot in (C) shows the M-CSF mean signal intensities of CD11b⁻ and CD11b⁺ AMs. Each dot
785 represents an individual cell.

786

787

788

789 **References**

790 Aegerter, H., Kulikauskaitė, J., Crotta, S., Patel, H., Kelly, G., Hessel, E.M., Mack, M., Beinke, S., and Wack, A. (2020). Influenza-induced monocyte-derived alveolar macrophages confer prolonged antibacterial protection. *Nature Immunology* 21, 145-157. 10.1038/s41590-019-0568-x.

791 Arts, R.J.W., Joosten, L.A.B., and Netea, M.G. (2016a). Immunometabolic circuits in trained immunity. *Seminars in Immunology* 28, 425-430. 10.1016/j.smim.2016.09.002.

792 Arts, R.J.W., Novakovic, B., Ter Horst, R., Carvalho, A., Bekkering, S., Lachmandas, E., Rodrigues, F., Silvestre, R., Cheng, S.-C., Wang, S.-Y., et al. (2016b). Glutaminolysis and Fumarate Accumulation Integrate Immunometabolic and Epigenetic Programs in Trained Immunity. *Cell metabolism* 24, 807-819. 10.1016/j.cmet.2016.10.008.

793 Bekkering, S., Arts, R.J.W., Novakovic, B., Kourtzelis, I., van der Heijden, C.D.C.C., Li, Y., Popa, C.D., Ter Horst, R., van Tuijl, J., Netea-Maier, R.T., et al. (2018). Metabolic Induction of Trained Immunity through the Mevalonate Pathway. *Cell* 172, 135-146.e139. 10.1016/j.cell.2017.11.025.

794 Brown, G.D. (2005). Dectin-1: a signalling non-TLR pattern-recognition receptor. *Nat Rev Immunol* 6, 33-43. 10.1038/nri1745.

795 Christ, A., Günther, P., Lauterbach, M.A.R., Duewell, P., Biswas, D., Pelka, K., Scholz, C.J., Oosting, M., Haendler, K., Baßler, K., et al. (2018). Western Diet Triggers NLRP3-Dependent Innate Immune Reprogramming. *Cell* 172, 162-175.e114. 10.1016/j.cell.2017.12.013.

796 Cirovic, B., de Bree, L.C.J., Groh, L., Blok, B.A., Chan, J., van der Velden, W., Bremmers, M.E.J., van Crevel, R., Handler, K., Picelli, S., et al. (2020). BCG Vaccination in Humans Elicits Trained Immunity via the Hematopoietic Progenitor Compartment. *Cell Host Microbe* 28, 322-334.e325. 10.1016/j.chom.2020.05.014.

797 Cohen, M., Giladi, A., Gorki, A.-D., Solodkin, D.G., Zada, M., Hladik, A., Miklosi, A., Salame, T.M., Halpern, K.B., David, E., et al. (2018). Lung Single-Cell Signaling Interaction Map Reveals Basophil Role in Macrophage Imprinting. *Cell* 175, 1031-1044.e1018. 10.1016/j.cell.2018.09.009.

798 Deerhake, M.E., Danzaki, K., Inoue, M., Cardakli, E.D., Nonaka, T., Aggarwal, N., Barclay, W.E., Ji, R.R., and Shinohara, M.L. (2021). Dectin-1 limits autoimmune neuroinflammation and promotes myeloid cell-astrocyte crosstalk via Card9-independent expression of Oncostatin M. *Immunity* 54, 484-498.e488. 10.1016/j.immuni.2021.01.004.

799 Divangahi, M., Aaby, P., Khader, S.A., Barreiro, L.B., Bekkering, S., Chavakis, T., van Crevel, R., Curtis, N., DiNardo, A.R., Dominguez-Andres, J., et al. (2021). Trained immunity, tolerance, priming and differentiation: distinct immunological processes. *Nat Immunol* 22, 2-6. 10.1038/s41590-020-00845-6.

800 Dove, D.E., Linton, M.F., and Fazio, S. (2005). ApoE-mediated cholesterol efflux from macrophages: separation of autocrine and paracrine effects. *Am J Physiol Cell Physiol* 288, C586-592. 10.1152/ajpcell.00210.2004.

801 Du, Z., Lin, J.R., Rashid, R., Maliga, Z., Wang, S., Aster, J.C., Izar, B., Sorger, P.K., and Santagata, S. (2019). Qualifying antibodies for image-based immune profiling and multiplexed tissue imaging. *Nat Protoc* 14, 2900-2930. 10.1038/s41596-019-0206-y.

802 Fesel, P.H., and Zuccaro, A. (2016). β -glucan: Crucial component of the fungal cell wall and elusive MAMP in plants. *Fungal genetics and biology : FG & B* 90, 53-60. 10.1016/j.fgb.2015.12.004.

803 Gautier, E.L., Shay, T., Greter, M., Jakubzick, C., Ivanov, S., Helft, J., Chow, A., Elpek, K.G., Gordonov, S., Mazloom, A.R., et al. (2012). Gene-expression profiles and transcriptional regulatory pathways that underlie the identity and diversity of mouse tissue macrophages. *Nat Immunol* 13, 1118-1128. 10.1038/ni.2419.

804 Gibbings, S.L., Thomas, S.M., Atif, S.M., McCubbrey, A.L., Desch, A.N., Danhorn, T., Leach, S.M., Bratton, D.L., Henson, P.M., Janssen, W.J., and Jakubzick, C.V. (2017). Three Unique Interstitial Macrophages in the Murine Lung at Steady State. *American journal of respiratory cell and molecular biology* 57, 66-76. 10.1165/rcmb.2016-0361OC.

805 Goltsev, Y., Samusik, N., Kennedy-Darling, J., Bhate, S., Hale, M., Vazquez, G., Black, S., and Nolan, G.P. (2018). Deep Profiling of Mouse Splenic Architecture with CODEX Multiplexed Imaging. *Cell* 174, 968-981.e915. 10.1016/j.cell.2018.07.010.

806 Gross, O., Gewies, A., Finger, K., Schafer, M., Sparwasser, T., Peschel, C., Forster, I., and Ruland, J. (2006). Card9 controls a non-TLR signalling pathway for innate anti-fungal immunity. *Nature* 442, 651-656. 10.1038/nature04926.

807 Guilliams, M., De Kleer, I., Henri, S., Post, S., Vanhoutte, L., De Prijck, S., Deswarthe, K., Malissen, B., Hammad, H., and Lambrecht, B.N. (2013). Alveolar macrophages develop from fetal monocytes that differentiate into long-lived cells in the first week of life via GM-CSF. *J Exp Med* 210, 1977-1992. 10.1084/jem.20131199.

808 Halstead, E.S., Umstead, T.M., Davies, M.L., Kawasawa, Y.I., Silveyra, P., Howyrlak, J., Yang, L., Guo, W., Hu, S., Hewage, E.K., and Chroneos, Z.C. (2018). GM-CSF overexpression after influenza a virus infection

847 prevents mortality and moderates M1-like airway monocyte/macrophage polarization. *Respiratory Research* 19,
848 3. 10.1186/s12931-017-0708-5.

849 Hussell, T., and Bell, T.J. (2014). Alveolar macrophages: plasticity in a tissue-specific context. *Nat Rev*
850 *Immunol* 14, 81-93. 10.1038/nri3600.

851 Jaitin, D.A., Adlung, L., Thaiss, C.A., Weiner, A., Li, B., Descamps, H., Lundgren, P., Blériot, C., Liu, Z.,
852 Deczkowska, A., et al. (2019). Lipid-Associated Macrophages Control Metabolic Homeostasis in a Trem2-
853 Dependent Manner. *Cell* 178, 686-698.e614. 10.1016/j.cell.2019.05.054.

854 Kalafati, L., Kourtzelis, I., Schulte-Schrepping, J., Li, X., Hatzioannou, A., Grinenko, T., Hagag, E., Sinha, A.,
855 Has, C., Dietz, S., et al. (2020). Innate Immune Training of Granulopoiesis Promotes Anti-tumor Activity. *Cell*
856 183, 771-785.e712. 10.1016/j.cell.2020.09.058.

857 Kalia, N., Singh, J., and Kaur, M. (2021). The role of dectin-1 in health and disease. *Immunobiology* 226,
858 152071. 10.1016/j.imbio.2021.152071.

859 Kaur, M., Bell, T., Salek-Ardakani, S., and Hussell, T. (2015). Macrophage adaptation in airway inflammatory
860 resolution. *European respiratory review : an official journal of the European Respiratory Society* 24, 510-515.
861 10.1183/16000617.0030-2015.

862 Kemp, S.B., Carpenter, E.S., Steele, N.G., Donahue, K.L., Nwosu, Z.C., Pacheco, A., Velez-Delgado, A.,
863 Menjivar, R.E., Lima, F., The, S., et al. (2021). Apolipoprotein E Promotes Immune Suppression in Pancreatic
864 Cancer through NF- κ B-Mediated Production of CXCL1. *Cancer Res* 81, 4305-4318. 10.1158/0008-
865 5472.CAN-20-3929.

866 Keren-Shaul, H., Spinrad, A., Weiner, A., Matcovitch-Natan, O., Dvir-Szternfeld, R., Ulland, T.K., David, E.,
867 Baruch, K., Lara-Astaiso, D., Toth, B., et al. (2017). A Unique Microglia Type Associated with Restricting
868 Development of Alzheimer's Disease. *Cell* 169, 1276-1290.e1217. 10.1016/j.cell.2017.05.018.

869 Kopf, M., Schneider, C., and Nobs, S.P. (2014). The development and function of lung-resident macrophages
870 and dendritic cells. *Nat Immunol* 16, 36-44. 10.1038/ni.3052.

871 Li, F., Piattini, F., Pohlmeier, L., Feng, Q., Rehrauer, H., and Kopf, M. (2022a). Monocyte-derived alveolar
872 macrophages autonomously determine severe outcome of respiratory viral infection. *Sci Immunol* 7, eabj5761.
873 10.1126/sciimmunol.abj5761.

874 Li, X., Wang, H., Yu, X., Saha, G., Kalafati, L., Ioannidis, C., Mitroulis, I., Netea, M.G., Chavakis, T., and
875 Hajishengallis, G. (2022b). Maladaptive innate immune training of myelopoiesis links inflammatory
876 comorbidities. *Cell* 185, 1709-1727.e1718. 10.1016/j.cell.2022.03.043.

877 Lloyd, C.M., and Marsland, B.J. (2017). Lung Homeostasis: Influence of Age, Microbes, and the Immune
878 System. 46, 549-561. 10.1016/j.immuni.2017.04.005.

879 Machiels, B., Dourcy, M., Xiao, X., Javaux, J., Mesnil, C., Sabatel, C., Desmeccht, D., Lallemand, F., Martinive,
880 P., Hammad, H., et al. (2017). A gammaherpesvirus provides protection against allergic asthma by inducing the
881 replacement of resident alveolar macrophages with regulatory monocytes. *Nat Immunol* 153, 256.
882 10.1038/ni.3857.

883 McCubbrey, A.L., Barthel, L., Mohning, M.P., Redente, E.F., Mould, K.J., Thomas, S.M., Leach, S.M.,
884 Danhorn, T., Gibbings, S.L., Jakubzick, C.V., et al. (2018). Deletion of c-FLIP from CD11bhi Macrophages
885 Prevents Development of Bleomycin-induced Lung Fibrosis. *American journal of respiratory cell and molecular
886 biology* 58, 66-78. 10.1165/rcmb.2017-0154OC.

887 Misharin, A.V., Morales-Nebreda, L., Reyfman, P.A., Cuda, C.M., Walter, J.M., McQuattie-Pimentel, A.C.,
888 Chen, C.-I., Anekalla, K.R., Joshi, N., Williams, K.J.N., et al. (2017). Monocyte-derived alveolar macrophages
889 drive lung fibrosis and persist in the lung over the life span. *J Exp Med* 214, 2387-2404. 10.1084/jem.20162152.

890 Mitroulis, I., Ruppova, K., Wang, B., Chen, L.-S., Grzybek, M., Grinenko, T., Eugster, A., Troullinaki, M.,
891 Palladini, A., Kourtzelis, I., et al. (2018). Modulation of Myelopoiesis Progenitors Is an Integral Component of
892 Trained Immunity. *Cell* 172, 147-161.e112. 10.1016/j.cell.2017.11.034.

893 Mould, K.J., Barthel, L., Mohning, M.P., Thomas, S.M., McCubbrey, A.L., Danhorn, T., Leach, S.M.,
894 Fingerlin, T.E., O'Connor, B.P., Reisz, J.A., et al. (2017). Cell Origin Dictates Programming of Resident
895 Versus Recruited Macrophages During Acute Lung Injury. *American journal of respiratory cell and molecular
896 biology*. 10.1165/rcmb.2017-0061OC.

897 Murdoch, J.R., and Lloyd, C.M. (2010). Chronic inflammation and asthma. *Mutation research* 690, 24-39.
898 10.1016/j.mrfmmm.2009.09.005.

899 Murphy, A.J., Akhtari, M., Tolani, S., Pagler, T., Bijl, N., Kuo, C.L., Wang, M., Sanson, M., Abramowicz, S.,
900 Welch, C., et al. (2011). ApoE regulates hematopoietic stem cell proliferation, monocytosis, and monocyte
901 accumulation in atherosclerotic lesions in mice. *J Clin Invest* 121, 4138-4149. 10.1172/JCI57559.

902 Novakovic, B., Habibi, E., Wang, S.-Y., Arts, R.J.W., Davar, R., Megchelenbrink, W., Kim, B., Kuznetsova, T.,
903 Kox, M., Zwaag, J., et al. (2016). β -Glucan Reverses the Epigenetic State of LPS-Induced Immunological
904 Tolerance. *Cell* 167, 1354-1368.e1314. 10.1016/j.cell.2016.09.034.

905 Quintin, J., Saeed, S., Martens, J.H.A., Giamarellos-Bourboulis, E.J., Ifrim, D.C., Logie, C., Jacobs, L., Jansen,
906 T., Kullberg, B.-J., Wijmenga, C., et al. (2012). *Candida albicans* Infection Affords Protection against

907 Reinfection via Functional Reprogramming of Monocytes. *Cell Host Microbe* 12, 223-232.
908 10.1016/j.chom.2012.06.006.

909 Rabe, K.F., and Watz, H. (2017). Chronic obstructive pulmonary disease. *Lancet (London, England)* 389, 1931-
910 1940. 10.1016/S0140-6736(17)31222-9.

911 Rathnayake, C.M., Metwali, N., Jayaratne, T., Kettler, J., Huang, Y., Thorne, P.S., O'Shaughnessy, P.T., and
912 Stone, E.A. (2017). Influence of rain on the abundance of bioaerosols in fine and coarse particles. *Atmos. Chem.
913 Phys.* 17, 2459-2475. 10.5194/acp-17-2459-2017.

914 Saeed, S., Quintin, J., Kerstens, H.H.D., Rao, N.A., Aghajanirefah, A., Matarese, F., Cheng, S.-C., Ratter, J.,
915 Berentsen, K., van der Ent, M.A., et al. (2014). Epigenetic programming of monocyte-to-macrophage
916 differentiation and trained innate immunity. *Science* 345, 1251086. 10.1126/science.1251086.

917 Schneider, C., Nobs, S.P., Kurrer, M., Rehrauer, H., Thiele, C., and Kopf, M. (2014). Induction of the nuclear
918 receptor PPAR- γ by the cytokine GM-CSF is critical for the differentiation of fetal monocytes into alveolar
919 macrophages. *Nat Immunol* 15, 1026-1037. 10.1038/ni.3005.

920 Serbina, N.V., and Pamer, E.G. (2006). Monocyte emigration from bone marrow during bacterial infection
921 requires signals mediated by chemokine receptor CCR2. *Nat Immunol* 7, 311-317. 10.1038/ni1309.

922 Shah, A., and Panjabi, C. (2014). Allergic aspergillosis of the respiratory tract. *European Respiratory Review*
923 23, 8-29. 10.1183/09059180.00007413.

924 Song, Y., Liu, J., Zhao, K., Gao, L., and Zhao, J. (2021). Cholesterol-induced toxicity: An integrated view of the
925 role of cholesterol in multiple diseases. *Cell Metab* 33, 1911-1925. 10.1016/j.cmet.2021.09.001.

926 Taylor, P.R., Tsoni, S.V., Willment, J.A., Dennehy, K.M., Rosas, M., Findon, H., Haynes, K., Steele, C., Botto,
927 M., Gordon, S., and Brown, G.D. (2007). Dectin-1 is required for beta-glucan recognition and control of fungal
928 infection. *Nat Immunol* 8, 31-38. 10.1038/ni1408.

929 Vornholz, L., and Ruland, J. (2020). Physiological and Pathological Functions of CARD9 Signaling in the
930 Innate Immune System. *Curr Top Microbiol Immunol* 429, 177-203. 10.1007/82_2020_211.

931 Wu, K., Byers, D.E., Jin, X., Agapov, E., Alexander-Brett, J., Patel, A.C., Cella, M., Gilfilan, S., Colonna, M.,
932 Kober, D.L., et al. (2015). TREM-2 promotes macrophage survival and lung disease after respiratory viral
933 infection. *J Exp Med* 212, 681-697. 10.1084/jem.20141732.

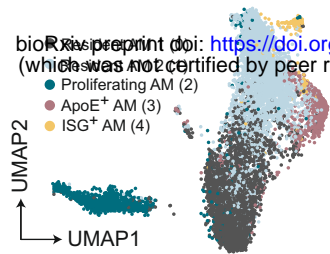
934 Yao, Y., Jeyanathan, M., Haddadi, S., Barra, N.G., Vaseghi-Shanjani, M., Damjanovic, D., Lai, R., Afkhami, S.,
935 Chen, Y., Dvorkin-Gheva, A., et al. (2018). Induction of Autonomous Memory Alveolar Macrophages Requires
936 T Cell Help and Is Critical to Trained Immunity. *Cell* 175, 1634-1650.e1617. 10.1016/j.cell.2018.09.042.

937 Yu, X., Buttigereit, A., Lelios, I., Utz, S.G., Cansever, D., Becher, B., and Greter, M. (2017). The Cytokine
938 TGF- β Promotes the Development and Homeostasis of Alveolar Macrophages. 1-15.
939 10.1016/j.immuni.2017.10.007.

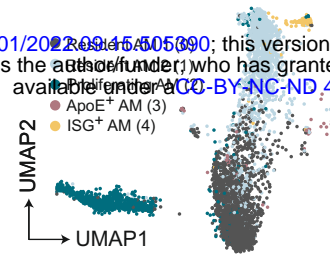
940 Zahalka, S., Starkl, P., Watzenboeck, M.L., Farhat, A., Radhouani, M., Deckert, F., Hladik, A., Lakovits, K.,
941 Oberndorfer, F., Lassnig, C., et al. (2022). Trained immunity of alveolar macrophages requires metabolic
942 rewiring and type 1 interferon signaling. *Mucosal Immunol.* 10.1038/s41385-022-00528-5.

943

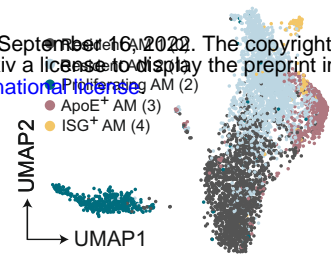
A Day 7, BALF, combined UMAP



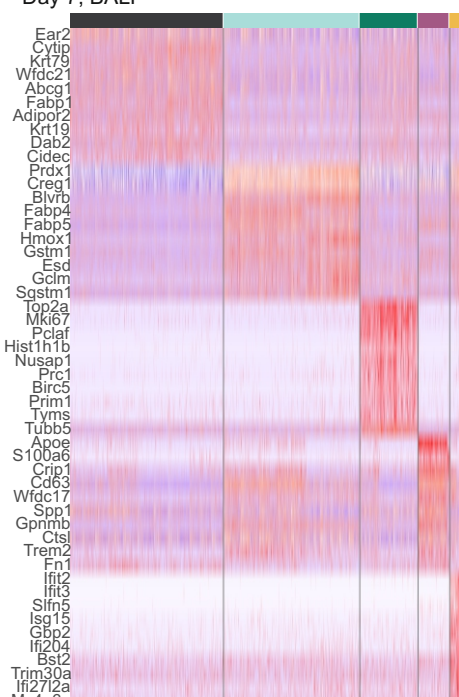
C Day 7, BALF, PBS



D Day 7, BALF, β -glucan

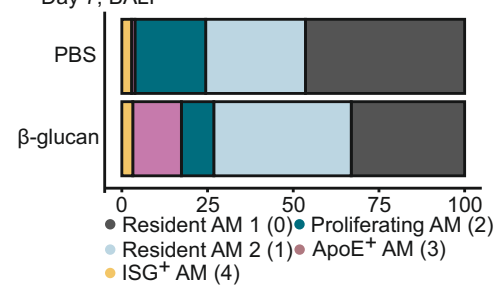


B Day 7, BALF

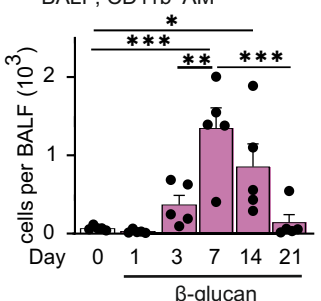


- Resident AM 1 (0) ● Proliferating AM (2)
- Resident AM 2 (1) ● ApoE+ AM (3)
- ISG+ AM (4)

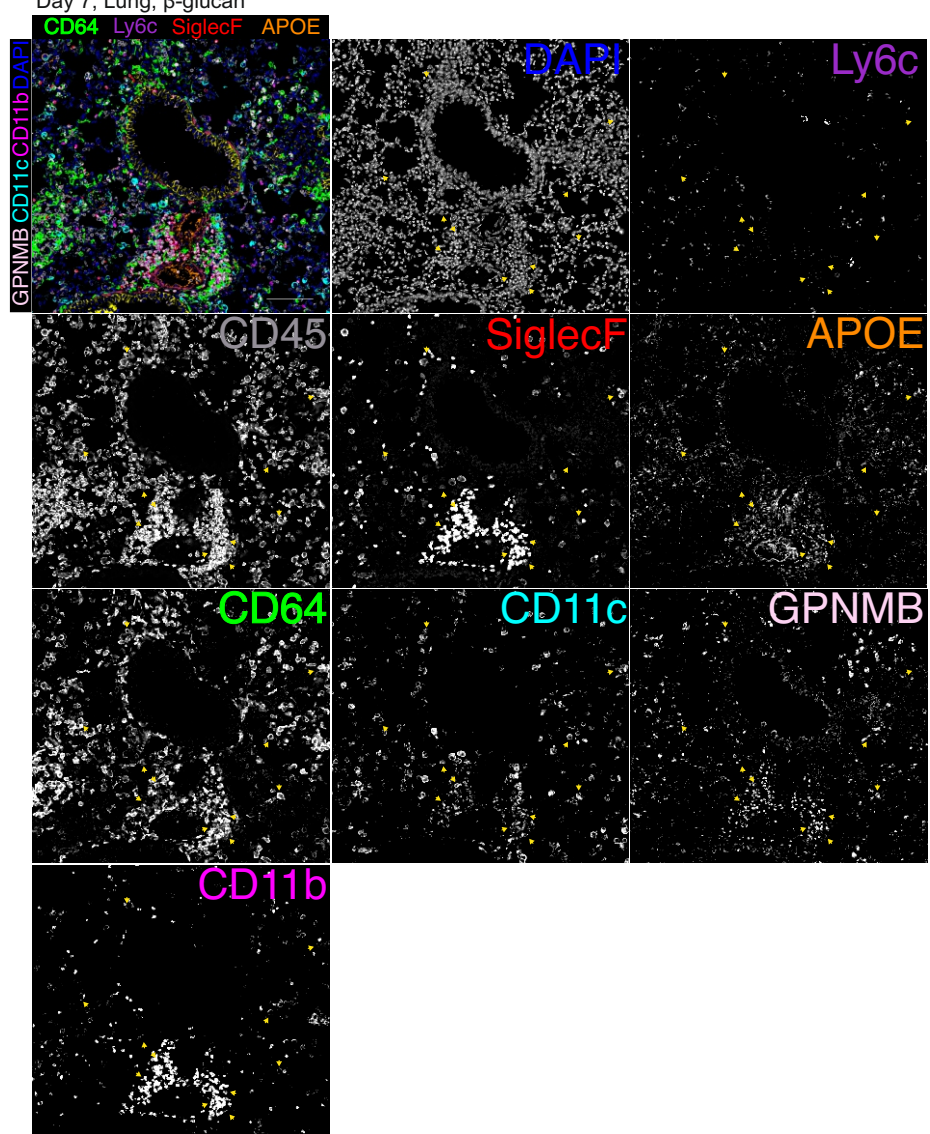
E Day 7, BALF

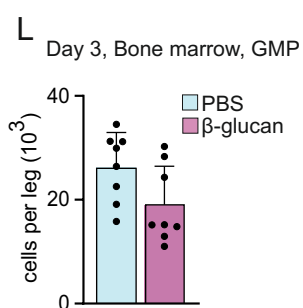
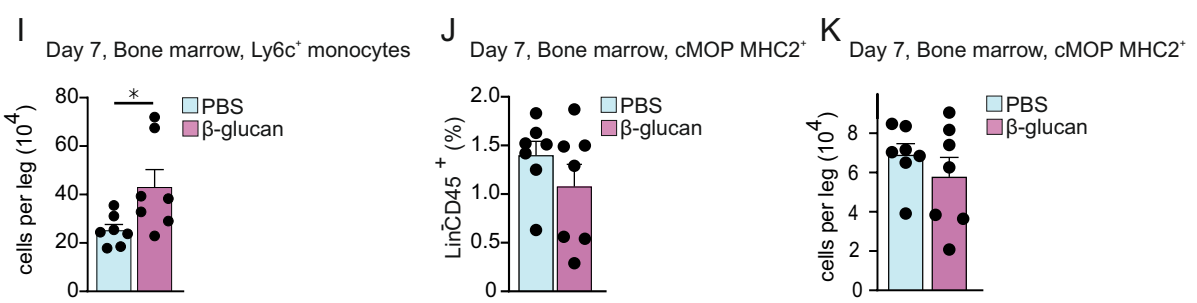
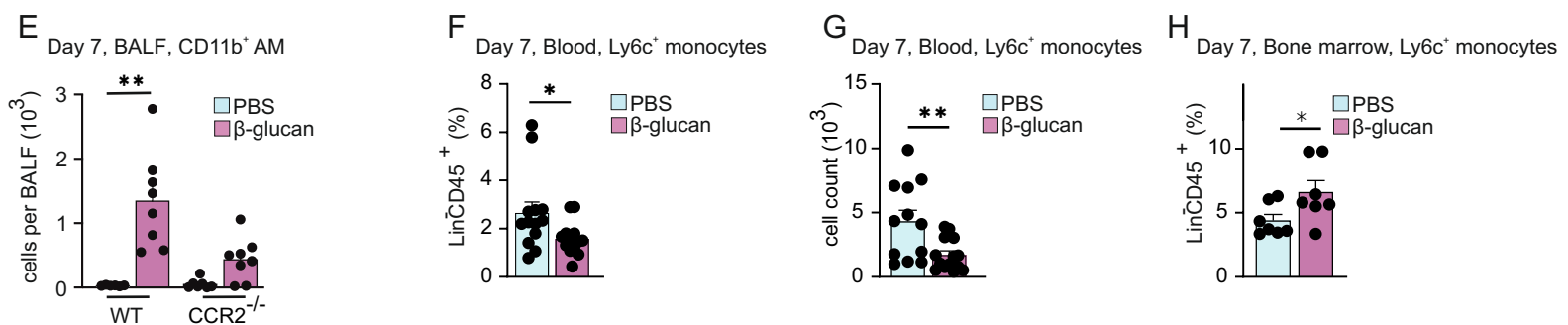
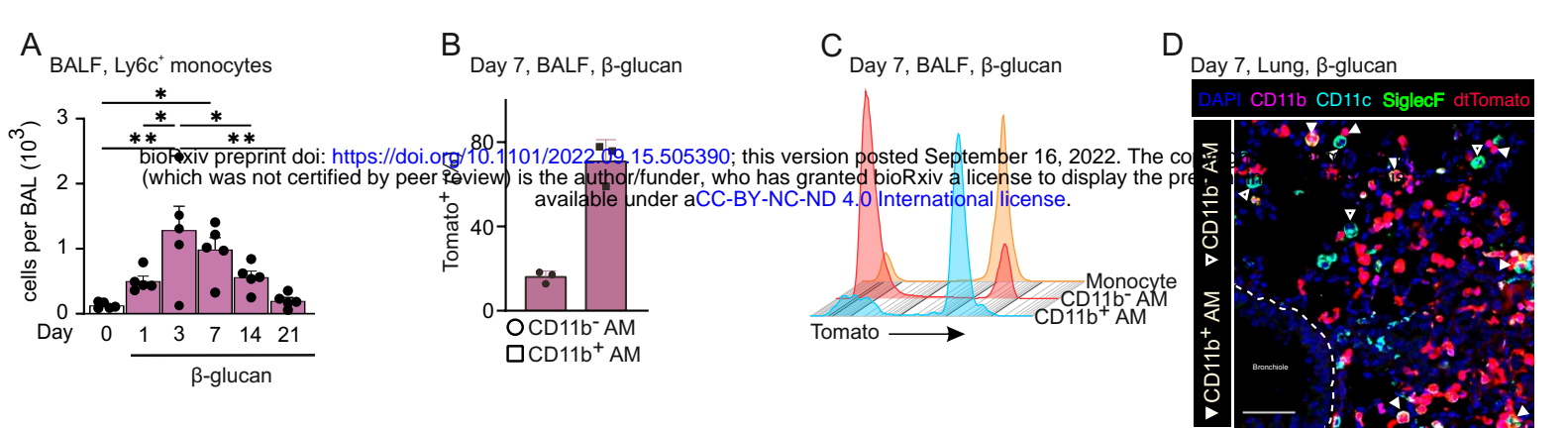


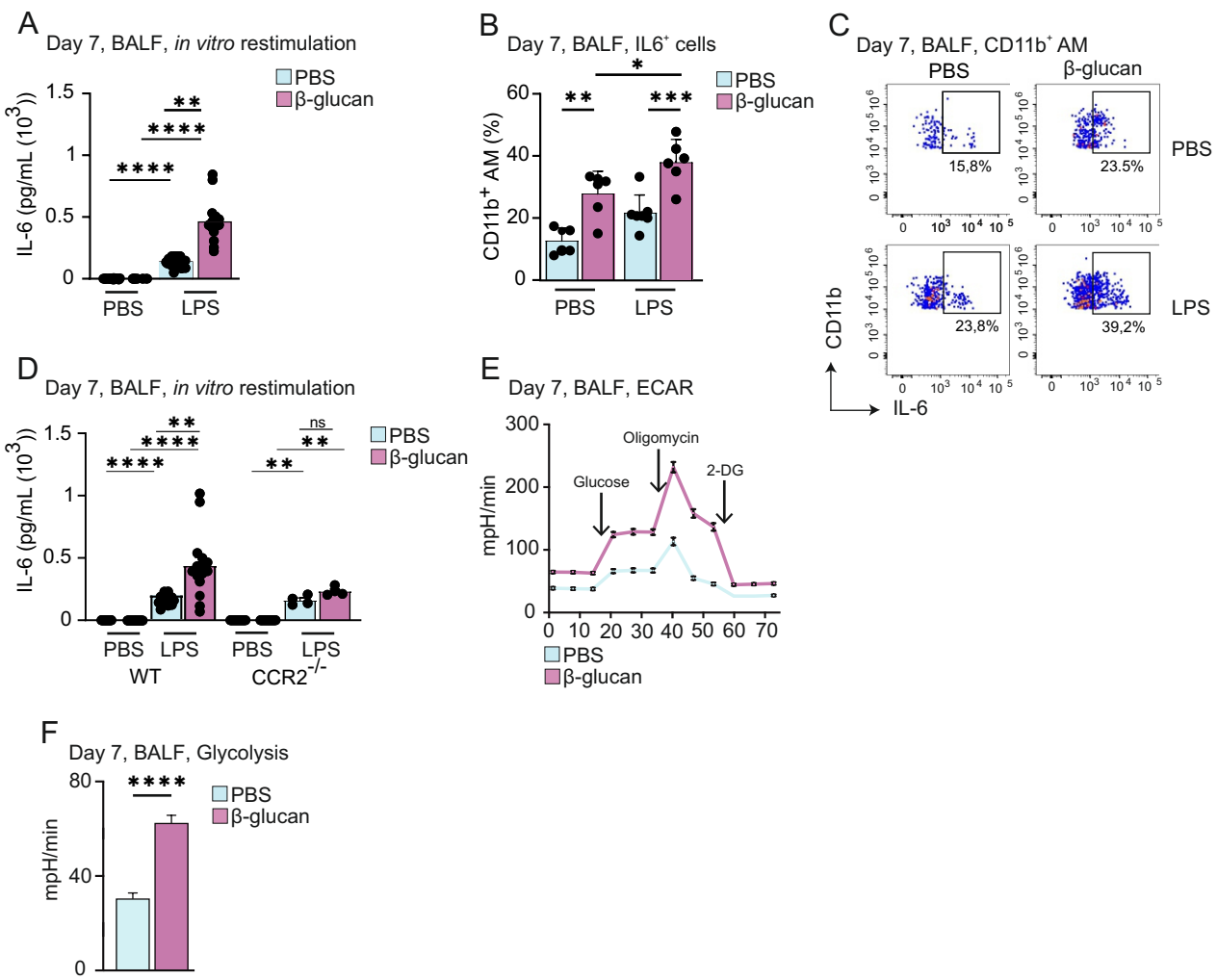
G BALF, CD11b+ AM



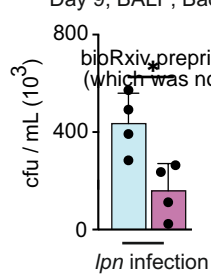
F Day 7, Lung, β -glucan



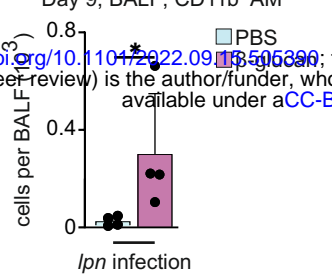




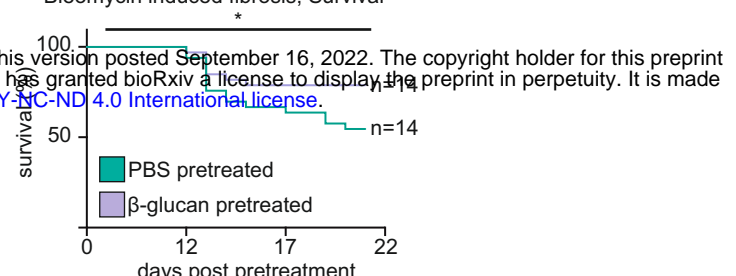
A Day 9, BALF, Bacterial load



B Day 9, BALF, CD11b⁺ AM

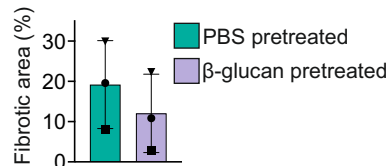


C Bleomycin induced fibrosis, Survival



D

Day 21, Bleomycin induced fibrosis, Lung



E

Day 21, Bleomycin induced fibrosis, Lung

